

RESEARCH

Open Access



Clinical-grade extracellular vesicles derived from umbilical cord mesenchymal stromal cells: preclinical development and first-in-human intra-articular validation as therapeutics for knee osteoarthritis

Aliosha I. Figueroa-Valdés^{1,6†} , Patricia Luz-Crawford^{2,6†} , Yeimi Herrera-Luna^{2,6} , Nicolás Georges-Calderón^{1,4,6} , Cynthia García^{2,4,6} , Hugo E. Tobar^{1,6} , María Jesús Araya^{2,4,6} , José Matas^{9,10}, Darío Donoso-Meneses^{1,4,6} , Catalina de la Fuente⁵, Jimena Cuenca^{1,5,6,13} , Eliseo Parra⁵, Fernando Lillo⁵, Cristóbal Varela¹¹, María Ignacia Cádiz^{1,5,13} , Rolando Vernal⁷ , Alexander Ortloff⁸ , Gino Nardocci^{3,6,15} , Verónica Castañeda^{3,4,6} , Catalina Adasme-Vidal^{1,6}, Maximiliano Kunze-Küllmer^{5,13,14} , Yessia Hidalgo^{1,6} , Francisco Espinoza^{5,6,9,12}, Maroun Khoury^{1,5,6,13,14*†}  and Francisca Alcayaga-Miranda^{1,5,6,13*†} 

Abstract

Osteoarthritis (OA) is a joint disease characterized by articular cartilage degradation. Persistent low-grade inflammation defines OA pathogenesis, with crucial involvement of pro-inflammatory M1-like macrophages. While mesenchymal stromal cells (MSC) and their small extracellular vesicles (sEV) hold promise for OA treatment, achieving consistent clinical-grade sEV products remains a significant challenge. This study aims to develop fully characterized, reproducible, clinical-grade batches of sEV derived from umbilical cord (UC)-MSC for the treatment of OA while assessing its efficacy and safety. Initially, a standardized, research-grade manufacturing protocol was established to ensure consistent sEV production. UC-MSC-sEV characterization under non-cGMP conditions showed consistent miRNA and protein profiles, suggesting their potential for standardized manufacturing. In vitro studies evaluated the efficacy, safety, and potency of sEV; animal studies confirmed their effectiveness and safety. In vitro, UC-MSC-sEV polarized macrophages to an anti-inflammatory M2b-like phenotype, through *STAT1* modulation, indicating their potential to create an anti-inflammatory environment in the affected joints. In silico studies confirmed sEV's immunosuppressive signature through miRNA and proteome analysis. In an OA mouse model, sEV injected intra-articularly (IA) induced hyaline

†Aliosha I. Figueroa-Valdés and Patricia Luz-Crawford have contributed equally to this study.

†Maroun Khoury and Francisca Alcayaga-Miranda have contributed equally to this study.

*Correspondence:

Maroun Khoury
mkhoury@uandes.cl
Francisca Alcayaga-Miranda
falcalyaga@uandes.cl

Full list of author information is available at the end of the article



cartilage regeneration, validated by histological and μ CT analyses. The unique detection of sEV signals within the knee joint over time highlights its safety profile by confirming the retention of sEV in the joint. The product development of UC-MSC-sEV involved refining, standardizing, and validating processes in compliance with GMP standards. The initial assessment of the safety of the clinical-grade product via IA administration in a first-in-human study showed no adverse effects after a 12 month follow-up period. These results support the progress of this sEV-based therapy in an early-phase clinical trial, the details of which are presented and discussed in this work. This study provides data on using UC-MSC-sEV as local therapy for OA, highlighting their regenerative and anti-inflammatory properties and safety in preclinical and a proof-of-principle clinical application.

Keywords Small extracellular vesicles, Exosomes, Osteoarthritis, Mesenchymal, Stem cells, Stromal cells, First-in-human, Manufacturing, Macrophage polarization

Graphical Abstract

Introduction

Osteoarthritis (OA) is the most prevalent progressive multifactorial joint disease and is characterized mainly by the deterioration and loss of articular cartilage. OA is one of the main sources of chronic pain and disability in developed countries, causing substantial costs to the health and employment welfare systems [22, 24, 51]. The knee is the most affected joint, accounting for almost four-fifths of the OA burden worldwide [14]. To date, knee OA does not have treatments capable of delaying cartilage deterioration or restoring the function of the articular cartilage, basing its treatment on the symptomatic control of pain and joint stiffness through multimodal approaches [32].

The pathogenesis of OA is intricate and heterogeneous, with low-grade chronic inflammation recognized as a pivotal process in its onset and progression [75]. Prominent features of OA include chronic synovitis and cartilage degeneration, and emerging evidence suggests that synovial inflammation precedes cartilage degeneration [88]. Macrophages in synovial tissue, particularly the pro-inflammatory M1-like subtype, play a crucial role in initiating, sustaining, and amplifying inflammation by releasing cytokines such as IL-1 β , IL-6, and TNF- α [19]. Conversely, M2-like macrophages, with an anti-inflammatory phenotype, secrete cytokines like IL-10, which are essential for tissue repair and inflammation resolution [19]. In patients with OA, synovitis is characterized by an increased number of M1-like macrophages that produce reactive oxygen species (ROS) [84,95], which contributes to inflammation, matrix dysregulation, and cartilage damage [44, 92]. The impact of ROS on chondrocytes has been extensively documented, demonstrating that oxidative stress induces

apoptosis in primary cartilage cells [27, 53]. In animal models of OA, reducing pro-inflammatory mediators and ROS levels ameliorates crucial pathophysiological aspects of OA, underscoring the control of inflammation and oxidative stress as a targeted therapeutic strategy for OA treatment [3, 41].

Mesenchymal stromal cells (MSC) have been widely studied as a possible biological therapy for OA, highlighting their clinical intra-articular (IA) application as a potential modality capable of halting or potentially reversing the degradation of articular cartilage in animal models [77]. This therapeutic effect has been intricately linked to small extracellular vesicles (sEV), which demonstrate similar paracrine tissue regenerative capabilities to their cellular counterparts while presenting a cell-free and safer product [39, 68, 86, 91]. In animal models of OA, therapies utilizing MSC-sEV have demonstrated promising preclinical efficacy by promoting cartilage regeneration and mitigating OA progression through the modulation of immune reactivity [96], restoring cartilage matrix homeostasis [98] and chondrogenic stimulation [12]. Therapeutic outcomes depend mainly on the origin of the parental cell [6]. Although there are no clinical reports of IA administration of MSC-sEV therapeutics in patients with OA, clinical cases of graft-versus-host disease [33] and chronic kidney disease [59] have reported good tolerability after systemic administration, which substantiates the ongoing early-stage clinical development of sEV-based therapeutics.

Pursuing standardized manufacturing protocols to produce clinical-grade products with defined critical quality attributes poses a significant challenge for clinical research groups. Ensuring consistency and reproducibility across diverse production batches remains paramount [67]. The governing principle of "the process is the product" necessitates stringent delineation, characterization, and oversight at every manufacturing phase, from initial parental tissue selection to the

ultimate packaging of the final product. This strict process design should integrate preclinical evidence and be meticulously formulated within a regulatory framework. Despite ongoing efforts, no clinical-grade sEV-based products have yet obtained market approval from regulatory agencies for any medical indication, including OA treatment.

According to our previously published data, the umbilical cord (UC) is the most promising source of MSC for treating OA due to its superior chondrogenic capacity and ability to suppress T-cell proliferation in vitro, along with lower angiogenic properties compared to bone marrow and other sources of placental origin [23]. The results were validated in a Phase I/II Randomized Controlled Clinical Trial and in a Phase I Dose Escalation Clinical Trial conducted in 2019 (NCT No. 02580695) [47, 48]. Given that the mechanism of action (MoA) underlying this therapy is highly associated with sEV, we aimed to develop a clinical-grade therapy based on UC-MSC-derived sEV to treat knee OA. The objective of this study is to investigate their efficacy and safety profile. To ensure consistent production of the therapeutic product, we initially developed a standardized research-grade manufacturing protocol. We extensively studied the efficacy, safety profile, and underlying MoA using various in vitro and in vivo experimental approaches. Subsequently, this manufacturing process underwent adaptation, homologation, and validation to adhere to good manufacturing practice (GMP) regulations, ensuring compliance with quality standards for clinical use. Finally, the clinical-grade product underwent its first safety assessment in human through IA administration of the knee joint. Our results showed a complete characterization of sEV derived from UC-MSC under non-cGMP conditions. We identified consistent miRNA and protein profiles across multiple batches, indicating the potential of a standardized manufacturing process. This research offers a comprehensive insight into the preclinical characterization and initial clinical application of UC-MSC-derived sEV as an IA therapy for OA, emphasizing their regenerative and anti-inflammatory properties and safety profiles, as well as proof-of-concept engineering of sEV to incorporate an exogenous miRNA cargo for delivery in key cell lineages involved in OA. The work presented here culminates in the design of an early-phase clinical trial that is poised and expected to begin enrollment immediately. This trial uses a defined dose-escalation protocol of UC-MSC-sEV for the treatment of knee OA. The primary objectives of this trial will be to evaluate safety, feasibility, and toxicity and to determine the optimal feasible dose for consecutive trials.

Materials and methods

Non-clinical (non cGMP) sEV production and enrichment

Preclinical sEV batches were obtained as reported previously [20]. Briefly, UC-MSC from three donors in passage 5 were seeded and expanded in a maintenance medium composed of Dulbecco's modified Eagle's medium (DMEM), high glucose, supplemented with 1% penicillin/streptomycin solution (10,000 U/mL and 10,000 µg/mL, respectively), 1% L-glutamine (200 mM) (all from Gibco, Paisley, United Kingdom), and 5% human platelet lysate (hPL) on 10-layer Nunc™ EasyFill™ Cell Factory™ systems (Thermo Fisher Scientific, Waltham, MA, United States, Cat. #140400) with a density of 6250 cells/cm². After cells reached ~70–80% confluence, the maintenance medium was discarded, and cells were washed three times with PBS 1X before addition of the induction media (DMEM high glucose + 1% L-Glutamine) for sEV production for 48 h. The recovered medium was clarified by serial centrifugations and filtrations. After obtaining the total supernatant (SN), the sEV were centrifuged at 100,000×g for 1 h at 4 °C, the SN was discarded, and the sEV were washed with PBS 1X. The suspension was then centrifuged at 100,000×g for 1 h at 4 °C. The SN was again discarded, and the precipitated sEV were resuspended in the remaining PBS 1X and then preserved at – 80 °C until use. Ethical approval for the donation of umbilical cords to obtain stem cells with a therapeutic purpose was obtained from the Scientific Ethical Committee of the public agency *Servicio de Salud Metropolitano Oriente* (CECSSMO050612) and written informed consent was obtained from the umbilical cord donor.

sEV characterization and staining

sEV characterization for size, concentration, identity, and purity assessment was performed according to MISEV guidelines [87], following the protocols previously described by our group [20] with no changes in the antibodies or equipment used. Briefly, the size mode (nm) and concentration (particles/mL) of the sEV preparations were assessed by nanoparticle tracking analysis (NTA) using a NanoSight NS300 system (Malvern Instruments Limited, United Kingdom), considering the sample dilution in the respective sEV suspension solution (PBS or Ringer Lactate). The presence of tetraspanins CD63, CD81, and CD9 (sEV surface markers), CD44 and CD90 (MSC origin markers) (BioLegend, United States of America, Cat. #397502 and Cat. #328102, respectively) and HLA DR/DP/DQ and HLA A/B/C (major histocompatibility complex class I and class II antigens, respectively) (BD Biosciences, United States of America, Cat. #564244 and eBioscience Cat. #14-9983-82) was evaluated by flow cytometry on a FACSCanto™ II cytometer (BD Biosciences, United States of America).

The acquired data were analyzed using FlowJo software (V10, BD, United States of America). The presence of Syntenin-1 (sEV endosomal origin marker), Flotillin-1 (sEV membrane marker), Calnexin (endoplasmic reticulum marker), and TOMM20 (mitochondria marker) was evaluated by western blot. The structure of sEV was evaluated by transmission electron microscopy (TEM) following a previously standardized protocol established by our group [20, 94]. Images were captured using a Talos™ F200C G2 (Scanning) TEM (Thermo Fisher Scientific) at the Advanced Microscopy Facility UMA-UC (Pontificia Universidad Católica de Chile, Santiago, Chile). sEV staining for in vitro and in vivo tracking was performed according to a previously established protocol by our group [20, 69] using the lipophilic near-infrared fluorescent cyanine dye DiR (Biotium, United States of America, Cat. #60017) as sEV-membrane staining agent and washed using MW 3000 size-exclusion exosome spin columns (Invitrogen, United States of America, Cat. #4484449) according to the manufacturer's instructions. The stained particles were analyzed using NTA as described previously [20].

sEV cargo characterization: miRNA profiling and proteomics

Three independent UC-MSC donors were selected for the production and enrichment of sEV. The obtained sEV were characterized by NTA to determine the size mode and particle concentration and by flow cytometry to evaluate CD63 expression as sEV marker (>90% of positive events). A value of 4×10^9 sEV particles of each UC-MSC donor was used for miRNA profiling and proteomics.

The sEV-miRNA cargo profile was determined using the services of FIRALIS S.A. (Huningue, France; www.firalis.com). Briefly, miRNA profiling was performed using HTG/EdgeSeq Whole Transcriptome Assay (WTA; 2083 miRNAs), followed by sequencing on an Illumina NextSeq 500. The data obtained were normalized before the comparative analyses. The miRNA enrichment percentages were calculated by considering the number of reads of a particular miRNA and the total number of reads in the sample.

For sEV-protein cargo identification, label-free quantification (LFQ) coupled with high-resolution mass spectrometry was performed at the Clinical Proteomic Platform of the Institute for Regenerative Medicine & Biotherapy of the University of Montpellier (Montpellier, France). For this purpose, sEV were lysed, and the proteins were reduced, alkylated, and digested with trypsin using magnetic beads. The peptides were desalted and injected into a nanoLC-Q-TOF Impact II (Bruker, United States of America). Protein identification was performed with Maxquant software (V1.6.17.0; Max Planck Institute

of Biochemistry, Germany). The parameters used were the following: trypsin as digestion enzyme, 1 as the number of missed cleavages, a tolerance of 10 ppm for parent ions and 0.05 Da for MS/MS spectra, the minimum peptide size was 5 amino acids, the maximum peptide mass was 4.600 Da and a protein identification false discovery rate (FDR) was set at 2.5%. The UniProt database was used as the reference (V01/02/2021). The initial protein amount normalized to LFQ intensities for each protein before data processing was performed using the LFQ-Analyst platform. Proteins that were considered contaminants and redundant were removed. LFQ data for each protein were transformed using the $\log_2(x)$ formula. The data were then normalized to a normal distribution and missing values were imputed using the BCPA (Bayesian missing value imputation) method.

In vitro biological activity of UC-MSC-sEV

Cell isolation and culture

For in vitro studies, human osteoarthritic chondrocytes (huOAC), synoviocytes, and monocytes were procured following established protocols, which were reviewed and approved by the Scientific Ethics Committee of Universidad de Los Andes (approval certificate #CEC2021077). Tissue samples were collected after obtaining written informed consent from the donors, adhering to the institutional guidelines of the Universidad de los Andes. The isolation and expansion of huOAC were performed using previously described methodologies [65]. Briefly, huOAC and synoviocytes were isolated from joint tissues of patients who underwent total knee or hip replacement surgery. The cartilage tissue for huOAC isolation was sectioned into thin slices and subjected to one hour-long digestion using a protease solution (Merck KGaA, Germany, Cat. #P5147) at 37 °C under continuous agitation. This was followed by secondary digestion in a collagenase II solution (Sigma-Aldrich, United States of America, Cat. #C6885) for 16 h at 37 °C under constant agitation. Synoviocytes were obtained by slicing the synovial membrane into approximately 1 mm² pieces and digesting them in a collagenase I solution (Sigma-Aldrich, United States of America, Cat. #C0130) under similar conditions. After digestion, huOAC and synoviocyte samples were filtered through a 40 µm cell strainer (FALCON, United States of America, Cat. #352340) to eliminate undigested tissue. The cells were cultured in DMEM supplemented with 10% fetal bovine serum (FBS; Gibco, United States of America, Cat. #10437028), 1% P/S, and 1% L-glut under standard culture conditions. Monocytes were derived from peripheral blood mononuclear cells obtained from healthy blood donors using Ficoll-Paque™ PLUS (Cytiva, Sweden, Cat. #171440002) following the manufacturer's instructions. Monocytes were

isolated using the EasySep™ Human Monocyte Isolation Kit (StemCell Technologies™, Canada, Cat. #19359) following the manufacturer's guidelines. Upon isolation, monocytes were cultured in Iscove's Modified Dulbecco's Medium (IMDM; Gibco, United States of America, Cat. #12440-053) supplemented with 10% FBS, 1% P/S, 1% L-glut, 20 mM HEPES (Gibco, United States of America, Cat. #15630080), 50 μM β-mercaptoethanol (Gibco, United States of America, Cat. #21985-023), and 1% MEM non-essential amino acids (Gibco, United States of America, Cat. #11140-050) under standard culture conditions. Additionally, macrophage colony-stimulating factor (M-CSF; 20 ng/mL) (BioTechne, R&D Systems, Cat. #216-MC) was immediately added to the culture media to induce monocyte-macrophage differentiation.

sEV internalization assays

The PKH26-stained sEV internalization assay in huOAC, synoviocytes and macrophages was performed as previously described with some modifications. Briefly, PKH26 (Sigma-Aldrich, United States of America, Cat. #PKH26GL)-stained sEV were added to the culture media of either huOAC, synoviocytes or macrophages (1×10^8 particles per 200,000 cells). After 24 h, the cells were fixed with 4% PFA and permeabilized with a PBS 1X+Triton X-100 0.1% solution for 10 min on vertical agitation. huOAC and synoviocytes were stained with phalloidin-Alexa Fluor 488 at a 1:600 dilution (Invitrogen, United States of America, Cat. #A12379) and macrophages were stained with anti-CD206 at a 1:500 dilution (Biolegend, United States of America, Cat. #321110). Finally, the cells were washed three times with PBS 1X before mounting on 12 mm glass slides using Fluoroshield with DAPI (Abcam, United States of America, Cat. #ab104139). Samples were left to dry at RT for at least 30 min, after which images were taken using a confocal microscope (SP8, Leica, Germany).

DiR-stained sEV internalization assay was performed in huOAC cells according to a previously established protocol by our group [2, 20, 69], with some modifications. Briefly, 10,000/well of huOAC were seeded in 4-well plates and cultured in 300 μL/well of DMEM supplemented with 10% FBS, 1% L-glut, and 1% P/S. After 24 h, cells were washed three times with PBS 1X, and a solution of 300 μL of DMEM (supplemented with 1% L-glut) containing DiR-stained sEV (35×10^3 particles per cell) was added per well. As an internalization control, a second 4-well replicate was cultured in parallel; however, once the sEV were added, they were incubated at 4 °C. After 16 h, cells were detached and analyzed by flow cytometry on a FACSCanto™ II cytometer (BD Biosciences, United States of America), and the data were analyzed using FlowJo software (V10, BD, United States

of America). For confocal microscopy imaging, huOAC (30,000 cells/well) were cultured on a 10 mm cover glass coated with Poly-L-Lysine in a 4-well plate. The cells were treated with 30×10^3 DiR-stained sEV/cell. Following a 16 h incubation period, huOAC were rinsed thrice with PBS 1X and fixed at room temperature (RT) for 30 min using 4% paraformaldehyde (PFA). Subsequently, nuclei were stained with Hoechst 33342 (Sigma Aldrich, United States of America, Cat. #63493) at a 1:2,000 dilution for 15 min at RT, and the samples were then mounted on a microscopy slide using fluorescence mounting medium (Dako, United States of America, Cat. # S3023). The acquired images were examined using a confocal microscope (SP8, Leica, Germany).

sEV loading with cel-miR-39

Engineered sEV were developed using electroporation to enrich them with a synthetic miRNA derived from *Caenorhabditis elegans* (cel-miR-39) (Ambion, United States of America, Cat. #4464076; Assay ID: MC20682). For this, sEV (2×10^9 particles) loaded with cel-miR-39 (360 nM) were resuspended in buffer containing sucrose (50 mM) (Sigma-Aldrich, United States of America, Cat. #S7903) in a total volume of 100 μL. Electroporation was performed using a single 4 mm cuvette in a Nucleofector electroporation system (Lonza, Germany, Cat. #AAF-1002B & AAF-1002X) following the ER-113 program. After electroporation, the sEV were incubated for 30 min at 37 °C for membrane stabilization. Subsequently, RNase A (Thermo Scientific, United States of America, Cat. #EN0531) was added to a final concentration of 5 μg/mL and incubated at 37 °C for another 30 min. The treated sEV were stored at -80 °C for at least 24 h before downstream analysis. Quantification of the miRNA loaded within the sEV involved: RNA extraction (TRIzol Reagent, Invitrogen, United States of America Cat. #15596026), reverse transcription (Applied Biosystems, United States of America, Cat. #43366596), qPCR (TaqMan, United States of America, Cat. #4440040), and miRNA cel-miR-39 TaqMan assay (Applied Biosystems, United States of America, Cat. #4427975; Assay ID: 464312_mat). The engineered sEVs' ability to transfer miRNA cargo was assessed on huOAC, synoviocytes and monocyte-derived macrophages by culturing them for 24 h with engineered sEV loaded with cel-miR-39 and sEV loaded with a scrambled sequence (Ambion, United States of America, Cat. #4464076; Assay ID: MC20682) was used as the control (15,000 particles/cell). Following the abovementioned protocols, RNA extraction, reverse transcription, and qPCR analyses were conducted to determine cel-miRNA-39 transference to cells.

Monocyte-derived macrophage polarization assay in vitro

Monocytes isolated from three healthy donors were used in a monocyte-derived macrophage (hmMØs) differentiation assay. Monocytes were seeded on a flat-bottom 96-well plate (100,000 cells/well) and cultured under standard conditions for 6–7 days in 250 µL of MLR medium (10% FBS, 1% P/S 1%, L-glut, 20 mM HEPES, 1% Non-Essential Amino Acid solution and 50 µM β-mercaptoethanol in Iscove's Modified Dulbecco's medium) supplemented with 20 ng/mL M-CSF (BioTechne, United States of America, Cat. #216-MC). Half of the cell culture medium was discarded every other day, and fresh MLR/M-CSF supplemented medium was added. After six days of culture, monocytes were differentiated into macrophages and characterized by flow cytometry using fluorophore-conjugated antibodies for CD68 and CD11b detection (both from BioLegend, United States of America, Cat. #333816 and Cat. #101206, respectively). At this point, sEV treatment was started at 1×10^8 sEV/well in MLR/M-CSF supplemented medium (100 µL). After 24 h, the SN was collected to study the cytokine secretion by macrophages using enzyme-linked immunosorbent assay (ELISA), and macrophages were detached to determine their polarization status by flow cytometry. The secreted Interleukin-10 (IL-10), Vascular endothelial growth factor (VEGF), Interleukin-6 (IL-6), Tumor necrosis factor-α (TNF-α), and Interleukin-1β (IL-1β) levels were determined by ELISA (Human DuoSet ELISA, R&D Systems, United States of America, Cat. #DY217B-05, DY293B-05, DY206-05, DY210-05, and DY201-05, respectively) following the manufacturer's instructions. To evaluate the polarization status of hmMØs, CD68 and CD11b were used to discriminate double-positive cells. Antibodies against HLA-DR (BD Biosciences, United States of America, Cat. #564244) and CD86 (BioLegend, United States of America, Cat. #305420) were used for pro-inflammatory immunophenotyping (M1 polarization markers), and antibodies for CD206 and CD163 detection (BioLegend, United States of America, Cat. #321110 and Cat. #333606) were used for anti-inflammatory immunophenotyping (M2 polarization markers). Normalization of the median fluorescence intensities (MeFI) of each M1 and M2 marker against the MeFI values obtained in no-treatment control macrophages was used to determine the polarization status of the cells: a higher proportion of HLA-DR and CD86 MeFI's in comparison to CD206 and CD163 MeFI's was an indicative of pro-inflammatory M1-like polarization; on the contrary, a higher fold change of CD206 and CD163 MeFI's in comparison to HLA-DR and CD86 was indicative of anti-inflammatory M2-like polarization. Cell viability staining (1:500, LIVE/

DEAD™ Fixable Near-IR Dead Cell Stain Kit; Invitrogen, United States of America, Cat. #L34975) was added to each sample for dead cell removal. Flow cytometry data acquisition was performed using a FACSCanto™ II cytometer (BD Biosciences, United States of America). The acquired data were analyzed using the FlowJo software (V10, BD, United States of America).

LDH-based cytotoxicity assay

Lactate dehydrogenase (LDH) release-based sEV cytotoxicity assessment was performed in huOAC following the manufacturer's instructions (Cytotoxicity Detection Kit^{PLUS}LDH; Roche, Germany, Cat. #04 744 926 001). Briefly, huOAC (2,900 cells/well) were plated on a 96-well flat-bottom cell culture plate and cultured in complete medium (100 µL/well; 10% FBS, 1% P/S 1% and L-glut in DMEM). After 24 h, the medium was replaced with fresh DMEM supplemented with 1% L-glut after three washes with PBS 1X, and sEV were added according to the following doses: dose 1 = 100×10^6 sEV/well; dose 2 = 400×10^6 sEV/well. After 24 h, SN was recovered to quantify LDH following manufacturer's instructions. The negative control corresponded to untreated huOAC, whereas the positive control corresponded to Triton X-100 treated huOAC.

Chondroprotective activity study

To evaluate the chondroprotective potential of sEV, menadione was used as a cell death-triggering agent in huOAC. For this purpose, huOAC (100,000 cells/well) were seeded in DMEM supplemented with 10% FBS, 1% P/S, 1% L-glut (300 µL/well) in a 24-well plate. Once 80% confluence was reached, 20 µM of menadione (Sigma-Aldrich, United States of America, Cat. #M5750-25G), and 1×10^8 sEV/well were added to fresh media (300 µL). Control wells without menadione, or menadione + sEV were also considered. After 6 h, PBS 1X containing 2% FBS (300 µL) was added to each well to wash and stop the menadione effect. Immediately, the SN was recovered and reserved, and the adherent cells were dissociated using TrypLE Express Enzyme (150 µL/well; Gibco, United Kingdom, Cat. #12605093). Next, PBS 1X containing 2% FBS (150 µL/well) was again added to recover the cells that may have remained attached to the wells. SN was centrifuged at $500 \times g$ for 5 min at 4 °C to obtain a cellular pellet for further evaluation of apoptosis using FITC Annexin V Apoptosis Detection Kit I (BD Pharmingen, United States of America, Cat. #556547) according to the manufacturer's instructions. For this, a mix of Annexin V (1.25 µL) and Propidium Iodide (2.5 µL) prepared in 50 µL of

Annexin V binding buffer was added per sample and incubated in darkness for 15 min at RT. Unstained, single-stained, and dead cells were used as controls. Flow cytometry data acquisition was performed using a FACSCanto™ II cytometer (BD Biosciences, United States of America), and the data were analyzed using FlowJo software (V10, BD, United States of America).

Evaluation of the therapeutic potential of sEV in vivo

Animals

All mice studies were performed at the Cells for Cells S.A. animal facility following protocols revised and approved by the Institutional Animal Care and Use Committee (IACUC) of the Universidad de los Andes (approval certificate #CEC2021077). C57BL/6j mice (The Jackson Laboratory; Cat. #000664) were bred and maintained in the same facility. Experiments were carried out using male and female mice aged 8 to 12 weeks, which were randomly assigned to groups according to the experimental design. Mice were housed in cages with *ad libitum* access to food and water, along with pleated paper and paper cones for environmental enrichment. To ensure animal welfare, a supervision protocol was implemented based on established guidelines [56]. This study complies with the ARRIVE Guidelines for reporting animal research, and a complete ARRIVE checklist is provided in Supplementary Checklist 1. No data was excluded in the analysis of the in vivo studies.

Collagenase-induced OA (CIOA) animal model

The collagenase-induced OA (CIOA) model was used as previously described [50, 81]. Three groups were established to be compared: (1) Sham (healthy control, no OA induction), (2) OA (CIOA) and (3) sEV (CIOA animals treated with sEV). For OA and sEV groups, one unit of type VII collagenase from *Clostridium histolyticum* (Sigma-Aldrich, United States of America, Cat. #C2399) in 5 μ L PBS 1X was IA administered to the knee joints of C57BL/6j mice on days 0 and 2. Additionally, for the sEV group, on days 7 and 14, the mice of sEV group were subjected to IA injections with 2×10^8 sEV diluted in 5 μ L PBS 1X. On day 42, the mice were euthanized, and paws were carefully dissected to remove soft tissues, followed by fixation in 4% PFA (Merck KGaA, Germany, Cat. #1004965000).

Micro-computed tomography of X-ray (μ CT) and histological evaluations

Paw samples were analyzed in a μ CT SkyScan 1278 (Bruker, United States of America) using the following parameters: 0.5 mm aluminum filter, 59 ± 4 kV, 500 μ A, 0.5° rotation and 360° angular range. The specimens were scanned in all spatial planes to obtain 2D and 3D

digitalized images using the Nrecon reconstruction software (V1.7.4.2; Bruker, United States of America). Then, standardized regions of interest (ROI) were obtained using the DATAVIEWER analyzer software (V1.5.6.2; Bruker, United States of America). The 2D (bone mineral density) and 3D (surface-to-volume ratio) bone changes in four knee zones (medial femur, lateral femur, medial tibia, and lateral tibia of each paw) were quantified using the CTan software (V1.18.4.1; Bruker, United States of America). Subsequently, the paws were decalcified through a two-week incubation in a 5% formic acid solution (prepared in distilled water; Merck KGaA, Germany, Cat. #100264) and embedded in paraffin for histological analysis. As previously described, tibias were sectioned frontally and stained with safranin O and Fast Green, as described for staining proteoglycans/cartilage and bone, respectively [76]. Cartilage degradation was quantified using a modified Pritzker/Osteoarthritis Research Society International (OARSI) score, as previously described [63, 81].

Immunogenic studies

For immunogenic analysis, three groups of mice were established: (1) sham, (2) OA and (3) sEV, as previously mentioned. Mice were IA injected with 5 μ L PBS 1X-solution containing $\sim 2 \times 10^8$ particles of UC-MSC-sEV. On day 10 (3 days after IA sEV administration), the popliteal lymph nodes were recovered and mechanically disaggregated. Then, cells were passed through a 40 μ m filter (Falcon, United States of America, Cat. #352340) and centrifuged at 1680 rpm for 6 min and cultured for 4 h with Phorbol 12-Myristate 13-Acetate (PMA, 50 ng/mL; Sigma-Aldrich, United States of America, Cat. #P8139) and ionomycin (1 μ g/mL; Sigma-Aldrich, Cat. #I0634) in the presence of 10 μ g/mL brefeldin A (Sigma-Aldrich, United States of America, Cat. #B6542). Subsequently, surface staining was performed using specific antibodies against CD4 (BioLegend, United States of America, Cat. #100422) and CD25 (Biolegend, United States of America, Cat. #102012), followed by fixation and permeabilization using Cytofix/Cytoperm™ (eBioscience, United States of America, Cat. #5523). Finally, intracellular staining for IFN- γ (BD Pharmingen, United States of America, Cat. #554411), IL-17 (BD Pharmingen, United States of America, Cat. #560666) and Foxp3 (eBioscience, United States of America, Cat. #125773–82) was achieved. Final acquisition was performed with a FACSCanto™ II cytometer (BD Biosciences, United States of America), and the data were analyzed using FlowJo software (V10, BD, United States of America).

sEV biodistribution study

To evaluate the in vivo biodistribution pattern of sEV therapeutics, mice were IA injected with 5 μ L-PBS 1X solution containing $\sim 2 \times 10^8$ particles of freshly purified DiR-stained sEV and non-stained sEV (auto-fluorescence control) ($n=3$ per group). At different time points after injection (0, 24, and 48 h), sEV fluorescence intensities were assessed using a LI-COR Odyssey imaging system (LI-COR Biosciences, United States of America) for the entire animal and excised organs according to the manufacturer's instructions. As control of the sEV staining procedure, DiR was diluted in 100 μ L PBS 1X (at a concentration of 71 μ M) and then washed using size-exclusion spin columns.

In silico studies

A comparative analysis of miRNAs within the sEV derived from UC-MSC donors was performed. To ensure analytical robustness, a threshold was implemented, wherein miRNAs with a count per million (CPM) greater than 0.5 in at least two out of three samples were considered. The identified miRNAs were subsequently cross-referenced with miRNet and HMDD databases [11, 15]. The target genes associated with the identified sEV-miRNAs were selected and subjected to Gene Ontology enrichment analysis, focusing on biological processes, using the R package GOSTats, GOchord, and networkD3 [18].

Concurrently, for protein analysis, proteins present in sEV with at least 2500 LFQ (protein abundance value) in at least two out of the three samples analyzed were considered. The resultant proteins were subjected to Gene Ontology enrichment analysis, specifically focusing on biological processes, using the R package GOSTats, GOchord, and networkD3.

To determine the effect of sEV on putative target genes, hmMØs were subjected to the polarization assay described before and RNA was extracted (TRIzol Reagent, Invitrogen, United States of America Cat. #15596026) for reverse transcription assay. Transcript levels of *STAT1* were determined by TaqMan assay (Applied Biosystems, United States of America, Cat. #4453320; Assay ID: Hs01013996_m1) and transcript levels of *PPAR γ* were determined by qPCR using Brilliant II SYBR Green (Agilent Technologies; Cat. #600828) and the following primers: forward 5'-CCTTGCAGTGGG GATGTCT-3'; reverse 5'-CTCGCCTTTGCTTTGGTC A-3'). Both qPCR were performed in an AriaMx Real-time PCR System (Agilent Technologies).

Formulation and stability studies in sEV-based product development

Formulation evaluations

For product development and process validation studies, three sEV batches were generated and isolated at a smaller scale using a previously described protocol, except for the utilization of either PBS 1X or Ringer Lactate (RL; Baxter, United States of America, Cat. #HRB2323) during the sEV washing step and the final sEV resuspension. Each formulation was evaluated according to the following parameters: particle's size mode (nm), concentration (particles/mL), identity markers (CD63, CD81, and CD9), and potency assays (via the hmMØs polarization assay), utilizing established protocols, as previously described. The stability assessment of the sEV-based therapeutics was conducted at 5 and 24 months after storage at -80 °C. This evaluation encompassed sEV batches produced and enriched on a reduced scale by employing RL as the vehicle for formulation.

Stability studies

Short-term stability of sEV products after thawing was conducted at 2–8 °C in previously -80 °C-stored sEV, which were thawed and maintained at 2–8 °C for 24 h. Both studies employed the same parameters as those previously described for evaluation.

Manufacture, quality controls and characterization of clinical grade UC-MSC-sEV

A flowchart of cells and sEV production for clinical use is illustrated in Supplementary Fig. 1.

Production of clinical grade UC-MSC

All tissue samples were obtained using protocols that were reviewed and approved by the Scientific Ethics Committee of the Universidad de Los Andes (approval certificate #CEC201861). Clinical grade cell manufacturing was carried out as previously described by our group with some modifications [30, 92348]. In brief, UC were obtained from full-term human placentas by cesarean section after signed informed consent from healthy donors following the United States of America (USA) Code of Federal Regulations (CFR) Food and Drug Administration (FDA) Title 21, Part 1271: Human Cells, Tissues, and Cellular and Tissue-Based Products, Subpart C: Donor Eligibility (§1271.45–1271.90). UC-MSC treatments were manufactured in a facility that complies with GMP in compliance with USA CFR FDA Title 21, part 1271, Subpart D: Current Good Tissue Practice (§1271.145–1271.320) and with International Organization for Standardization (ISO) certification for the Quality Management System (ISO Standard No. 9001:2015) of

the UC-MSC production process at Cells for Cells S.A., Santiago, Chile (www.c4c.cl). All sterility controls were negative to approve the subsequent use of UC-MSC.

UC-MSC were cryopreserved in the third passage ($p=3$) until their approval as the master cell bank (MCB) and were subsequently used in the clinic. Cell culture was performed as previously described [20, 30, 9, 48]. The UC-MSC were characterized according to the guidelines of the International Society for Cell and Gene Therapy [16]. Immunophenotyping of UC-MSC was performed using a Human MSC Analysis Kit (BD Stemflow™, United States of America, Cat. #562245), and dead cells were discarded using Zombie Aqua Dye (BioLegend, United States of America, Cat. #77143). The analysis was performed by flow cytometry using a FACSCanto™ II cytometer. The acquired data were analyzed using the FlowJo software V10. This analysis was performed using MCB cells to approve the lot for clinical use. The trilineage differentiation capacity of cultured UC-MSC was evaluated using the StemPro™ differentiation kits (Gibco, Life Technologies Corp., United States of America) following the manufacturer's instructions: Adipogenesis Kit (Cat. #A1007001), Chondrogenesis Kit (Cat. #A1007101) and Osteogenesis kit (Cat. #A1007201). After 21 days, cell differentiation into adipocytes was confirmed by Oil Red O staining of lipidic vacuoles (Sigma-Aldrich, United States of America, Cat. #O0625) and osteocyte differentiation was confirmed by calcium deposits detected using Alizarin Red staining (Sigma-Aldrich, United States of America, Cat. #A3757). Chondrogenic differentiation was confirmed after 10 days by Safranin O staining (Sigma-Aldrich, United States of America, Cat. #S2255). Tumorigenic tests of UC-MSC in immunocompromised mice were performed under specific pathogen-free conditions at the Cells for Cells S.A. animal facility. After 3 months, organs were collected (skin, liver, lung, brain, and kidney), and histopathological analysis was performed. The previously described results showed the absence of tumors. The genomic stability of the UC-MSC over time was tested by karyotype analysis of cells at p-5 according to the USA CFR FDA Title 21, Part 211: Current Good Manufacturing Practice for Finished Pharmaceuticals, Section 110: Sampling and testing of in-process materials and drug products (§210.110). Thus, a Batch Approval Certificate (BAC) is generated, as shown in Supplementary Fig. 2.

Clinical grade sEV production and quality controls

UC-MSC approved for clinical use were thawed and seeded in maintenance medium composed of DMEM (Corning, Mediatech Inc., United States of America, Cat. #15-018-CV), supplemented with 1% P/S, 2 mmol/L L-glut and 5% fibrinogen-depleted hPL (manufactured

by Cells for Cells S.A., under GMP compliance standard) [20], on a Nunc™ TripleFlask™ at a density of 2000 cells/cm². After the cells reached confluence, they were expanded and seeded on a 10-layer Nunc™ EasyFill™ Cell Factory™ system. After the cells reached approximately 80% confluence, the maintenance medium was discarded. Cells were washed with PBS 1X (Gibco, Life Technologies Corporation, United States of America, Cat. #10010072) before the addition of the induction medium for sEV production: DMEM supplemented with only 2 mmol/L L-glut. After 2 and 4 days, SN was collected and subjected to serial centrifugation to remove cellular debris and sequential filtrations in 0.45 and 0.22 μm pore-size membrane filtration units (Thermo Fisher Scientific, United States of America, Cat. #569-0020 and Cat. #566-0020, respectively), and then, subjected to serial ultracentrifugation (Thermo Electron LED GmbH, model Sorvall WX+) at 100,000×g for 70 min at 4 °C. The pellet obtained was washed once with RL, the supernatant was discarded and sEV were resuspended in the remaining RL, aliquoted, and stored at – 80 °C until use. The sterility of sEV was evaluated using the same protocol described above for the UC-MSC sterility assessment. Each final product of the sEV-based therapeutic for clinical use complied with standardized procedures based on GMP and all quality controls mentioned above.

First-in-human application of cGMP-sEV therapy for OA: sterility assessment, patient recruitment, and imaging protocols

For the clinical case, the selection of the clinical exploration dose was not established using the conventional allometric scaling method for human-equivalent dose (HED) typically used for small-molecule drugs. This, due to the limitations inherent to the complex manufacturing of an sEV-based product that imposes a limit on the dose of the product that can be produced, thereby restricting the range of doses feasible to administer in a clinical experience. Instead, the IA dose extrapolation for the HED was based on an evaluation of the observed preclinical and clinical efficacy of previous studies performed by our group using the sEV parental cells [47, 48], as well as an assessment of the acceptable safety risk, by the FDA's statement "If available, previous clinical experience with the cellular and gene therapy (CGT) product or related products, even if by a different route of administration or for a different condition, may help to justify the clinical starting dose," from the "Considerations for the Design of Early-Phase Clinical Trials of Cellular and Gene Therapy Products" guidance [17]. The exploratory dose was calculated based on our published clinical results of IA use of 2×10^6 UC-MSCs in knee OA [47] (NCT No. 03810521) and our own findings indicating a secretion

rate of $\sim 5.3 \times 10^{10}$ particles sEV of the same number of cells [20]. Considering the manufacturing feasibility of the sEV-based product, we estimate that a dose of $2 \times 10^{10} \pm 0.5 \times 10^{10}$ total sEV would be required for local administration to the knee.

The cGMP-sEV ($2 \times 10^{10} \pm 0.5 \times 10^{10}$ particles) packed into a syringe was kept at 4 °C until IA administration in the patient. The final number of particles was determined using NTA as described above. As a UC-MS-C-sEV therapeutic sterility assessment, 11×10^7 particles were used for contamination determination by Aerobic/anaerobic automated blood culture system, and 14×10^7 particles were used for endotoxin determination as described previously. Both control groups were negative for release of the final product. A Certificate of Analysis (CoA) was delivered, indicating that cGMP-sEV-based therapy has the necessary sEV characteristics for release and the minimum sterility requirements for patient administration (Supplementary Fig. 3).

The patient was recruited in October 2021 at the Osteoarthritis Center at the Clínica Universidad de los Andes in Santiago, Chile. Approval was obtained from the Scientific Ethical Committee of the public agency *Servicio de Salud Metropolitano Oriente* (CECSSMO030821). Written informed consent was obtained from the patient. Subject met the following inclusion criteria: age between 30 and 75 years, symptomatic knee OA (defined as daily pain at the affected joint for at least 3 months before inclusion and a visual analog scale equal to or greater than 40 mm), and grade II to III Kellgren-Lawrence radiographic changes. None of the following conditions was retained: meniscal rupture, bilateral symptomatic knee OA, disease of the hip and/or spine, local or systemic infection, any form of secondary arthritis, or previous malignancy. The injection was performed by an orthopedic surgeon at the superior lateral aspect of the patella using a 21-gauge, 1-inch needle. No local anesthetic was used before the puncture. Clinical outcomes (VAS and WOMAC indexes) were evaluated at 3, 6, and 12 months of follow-up.

Regarding the imaging procedure, MRI at baseline and 6 months later was analyzed by a blinded radiologist. The patient was studied using a Philips Achieva 3 Tesla MRI scanner, with Smart Knee software to achieve equal knee positioning in pre- and post-treatment resonance imaging. The MRI protocol aims to study articular cartilage volumetry to evaluate the positive changes with treatment and the absence of structural damage to the cartilage. The DICOM files were anonymized and sent electronically to a third party via a secure platform (Image Analysis Group—IAG—, London, UK) for analysis. The external company utilized proprietary software following ISO13485 and the USA CFR FDA Title 21, Part

11: Electronic Records; Electronic Signatures (§11.1–11.300), to perform Quality Controls on, segment, and quantify all MRI images. The images were analyzed by an IAG radiologist and reported to our group.

Phase I clinical trial design

The clinical investigation will represent a phase I trial focusing on UC-MS-C-sEV in patients with symptomatic Kellgren II-III knee OA. The phase I component of the study will be an open-label dose escalation pilot study (NCT No. 06431152; title: “Administration of sEV derived from UC-MS-C in patients with osteoarthritis of the knee: safety determination in a pilot dose-escalation study”) in which three cohorts of subjects with OA will receive increasing doses of UC-MS-C-sEV administered as a single IA injection. Each cohort will comprise four participants. Specifically, patients within the cohorts will be administered the following exploration doses: 2×10^9 particles/3 mL RL $\pm 0.5 \times 10^9$ particles (first cohort-low dose), 6×10^9 particles/3 mL RL $\pm 0.5 \times 10^9$ particles (second cohort-median dose), or 2×10^{10} particles/3 mL RL $\pm 0.5 \times 10^9$ particles (third cohort-high dose). Eligible study subjects will be enrolled at the Clínica Universidad de los Andes. The selection of the study subjects will be performed following the inclusion and exclusion criteria shown in Fig. 8E.

The UC-MS-C-sEV will be prepared at the Cells for Cells S.A. GMP facility based at the Clínica Universidad de los Andes. The sEV-based therapeutic for clinical use will be manufactured in compliance with standardized procedures based on GMP regulations and all quality controls aforementioned. The sEV therapeutic will be transported to the patient administration site under controlled conditions, ensuring maintenance of a temperature range between 2–8 °C. The sEV injection is expected to be administered within the first 6 h of product manufacture.

The primary study endpoints of this trial will focus on the safety, feasibility, and toxicity of the sEV-based product. The phase I will examine: (1) the incidence of immediate post-infiltration adverse reactions in patients; (2) the occurrence of synovitis post-infiltration in patients at 24 and 48 h, as well as on days 7 and 15; (3) the frequency of post-infiltration pain reported by patients at 24 and 48 h, and on days 7 and 15; and (4) the prevalence of adverse events related to sEV therapy occurring beyond IA infiltration at 24 and 48 h, and on days 7 and 15, as well as at months 2, 4, 6, 8, 10, and 12. The secondary study endpoint will be determine the optimal dose for phase II trials. The criteria that will be considered are: (1) Safety profile at infiltration at 24 and 48 h, and on days 7 and 15, as well as at months 2, 4, 6, 8, 10, and 12; (2) changes in WOMAC scores at months 2, 4, 6, 8, 10, and

12; and (3) alterations in the VAS pain scores at months 2, 4, 6, 8, 10, and 12.

Statistical analysis

All figure legends include *n* involved. Analyses were performed using GraphPad Prism (V10.2.0; United States of America). For the data normality test, a Shapiro–Wilk test was performed, followed by one-way ANOVA with Tukey’s multiple comparisons test or unpaired Student’s *t*-test, depending on the number of groups to be evaluated. For large datasets, outliers were removed using the robust regression and outlier removal (ROUT) method ($Q=1\%$). For non-parametric data, a Kruskal–Wallis test followed by Dunn’s multiple comparison post-test was performed. For in vivo model, there were no criteria set for including/excluding animals. P-values <0.05 were considered significant in all cases (* $p < 0.05$, ** $p < 0.01$, *** $p < 0.001$, **** $p < 0.0001$, ns: not significant).

Results

Characterization of UC-MSC-derived sEV therapeutics generated in non-cGMP conditions

Analysis of identity, purity, and morphology of UC-MSC-sEV

MSC from four UCs were individually enriched and characterized following ISCT recommendations [16] for their subsequent validation and use as sEV-producing parental cells (Supplementary Fig. 4). Thirty-nine batches of purified sEV were obtained under non-cGMP conditions using a protocol established, optimized, and validated in our facility and based on previous studies [2, 20, 69, 94]. Figure 1A illustrates the characterization of the sEV batches according to the MISEV guidelines (size, concentration, identity and purity markers, and morphology) [79, 87]. Specifically, NTA obtained data showed a unimodal size distribution (Fig. 1B), a mean of 149.4 ± 23.98 nm as size mode (Fig. 1C) and a concentration of $1,22 \times 10^{11} \pm 7,58 \times 10^{10}$ particles/mL (Fig. 1D). Bead-based flow cytometry analysis was performed to assess the presence of the tetraspanins CD63, CD81, and

CD9, which are considered classical sEV identity markers. The median fluorescence intensity (MeFI) of the gathered data showed the presence of all three markers. However, a hierarchy was identified in the detected MeFI, with CD63 being the most expressed (16.95 ± 12.05 a.u.), followed by CD81 (8.50 ± 5.65 a.u.), and CD9 (4.63 ± 2.78 a.u.) (Fig. 1E). The presence of MSC surface markers CD90 and CD44 was also evaluated to verify the MSC origin of the sEV (MeFI for CD90 = 24.17 ± 18.17 a.u.; MeFI for CD44 = 31.40 ± 36.01 a.u. (Fig. 1F), as well as the presence of HLA A/B/C major histocompatibility complex (MHC) class-I antigens (MeFI = 2.46 ± 2.14 a.u.) and the absence of HLA DR/DP/DQ MHC-class II antigens (MeFI = 1.15 ± 0.07 a.u.) (Supplementary Fig. 5). Western blot was performed to evaluate Syntenin-1 and Flotillin-1 as complementary identity markers and Calnexin and TOMM20 as sEV purity markers. As expected, the bands confirmed the presence of Syntenin-1 (sEV endosomal origin marker) and Flotillin-1 (sEV membranous component marker) and the absence of Calnexin (endoplasmic reticulum marker) and TOMM20 (mitochondrial marker) (Fig. 1G). TEM allowed the visualization of isolated particles composed of non-agglomerated, cup-shaped vesicles, with a size and morphology compatible with sEV (Fig. 1H). These data confirm the extracellular vesicle and exosome nature of UC-MSC’s secreted particles. These findings further confirm that sEV batches, purified according to our established protocol, align with MISEV guidelines, ensuring size, identity, and purity criteria and establishing their MSC origin.

miRNA and proteomic profiling of UC-MSC-sEV

Approximately 1604 distinct miRNAs were identified among sEV samples (1278 in sample sEV^{donor 1}, 1194 in sample sEV^{donor 2}, 1218 in sample sEV^{donor 3}, and 1220 in a biological replicate sample of sEV from donor 3) (Table S1). Notably, 904 miRNAs were shared among the sEV samples derived from three UC-MSC donors (Fig. 1I), indicating that they were commonly expressed

(See figure on next page.)

Fig. 1 UC-MSC secretes sEV with unique and reproducible molecular cargo. **A** Diagram of the sEV characterization and the associated methodology. Next, graphs depicting the: **B** size distribution, **C** size mode, and **D** concentration from NTA of isolated particles. **E** Representative histograms from bead-based flow cytometry analyses and MeFI fold change for sEV surface markers CD63, CD81 and CD9, and **F** representative histograms from bead-based flow cytometry analyses and MeFI fold change to detect the presence of UC-MSC origin markers CD90 and CD44 in sEV. **G** A representative western blot of MSC’s cell lysate and three independent sEV isolations is shown for determining the presence of sEV markers Syntenin-1 and Flotillin-1 as well as purity markers Calnexin and TOMM20. **H** A representative TEM micrograph of isolated sEV showing the classical “cup-shape” morphology adopted by the vesicles with this technique. **I** Venn diagram showing the distribution of identified sEV-miRNA among three UC-MSC donor (plus a biological replicate of one of them). **J** Mean percentage distribution of top expressed miRNAs identified in sEV. **K** Venn diagram displaying the number of proteins identified in sEV derived from three different UC-MSC donors. Box and whiskers plot (solid lines = median); a.u. = arbitrary units; outliers were removed by ROUT method, $Q = 1\%$; $n = 40$ for: size mode, concentration, CD63, CD81 and CD9 determination (UC-MSC donors = 5); $n = 4$ for CD90 and CD44 (UC-MSC donors = 4). Percentages in representative histograms refers to the bead population

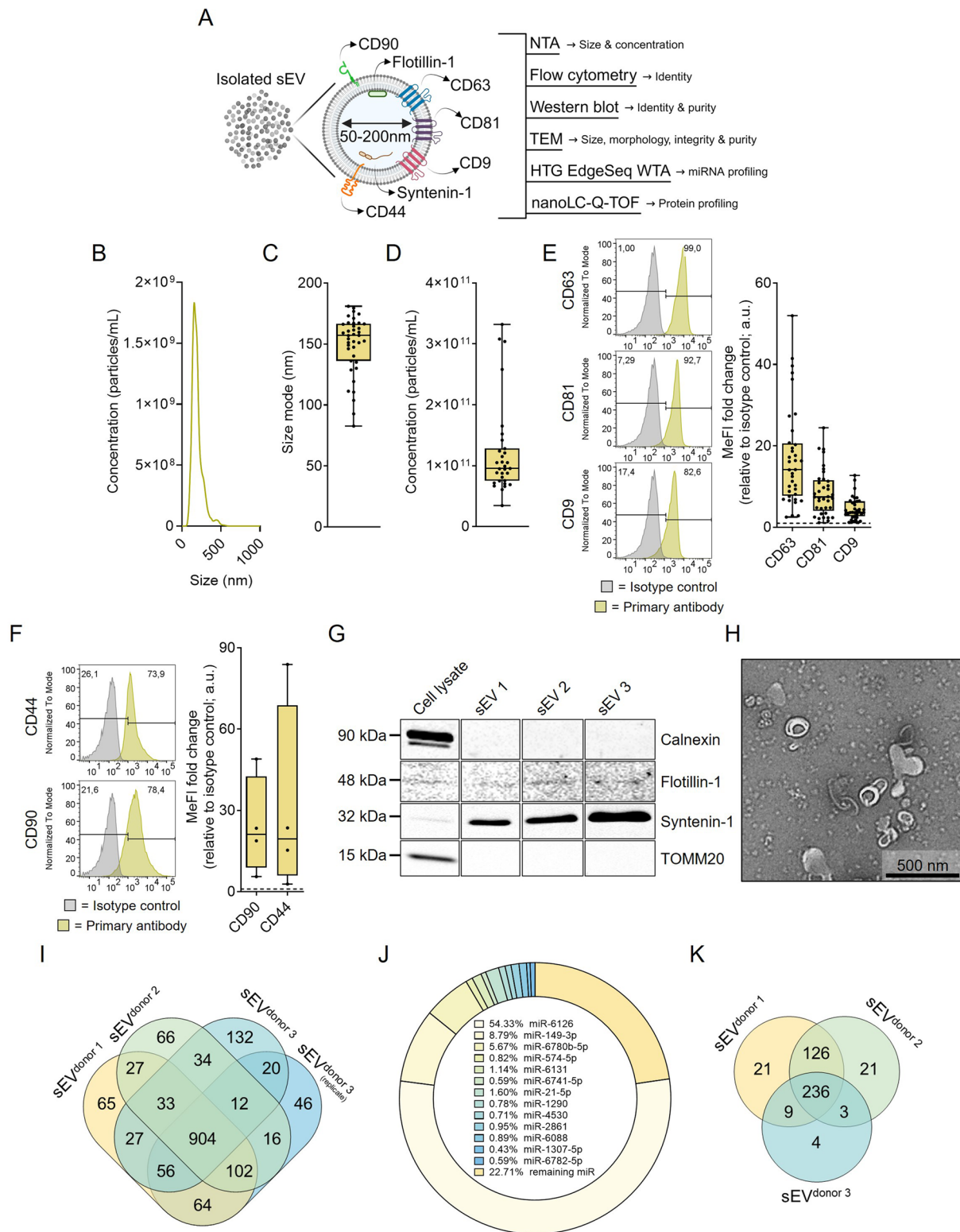


Fig. 1 (See legend on previous page.)

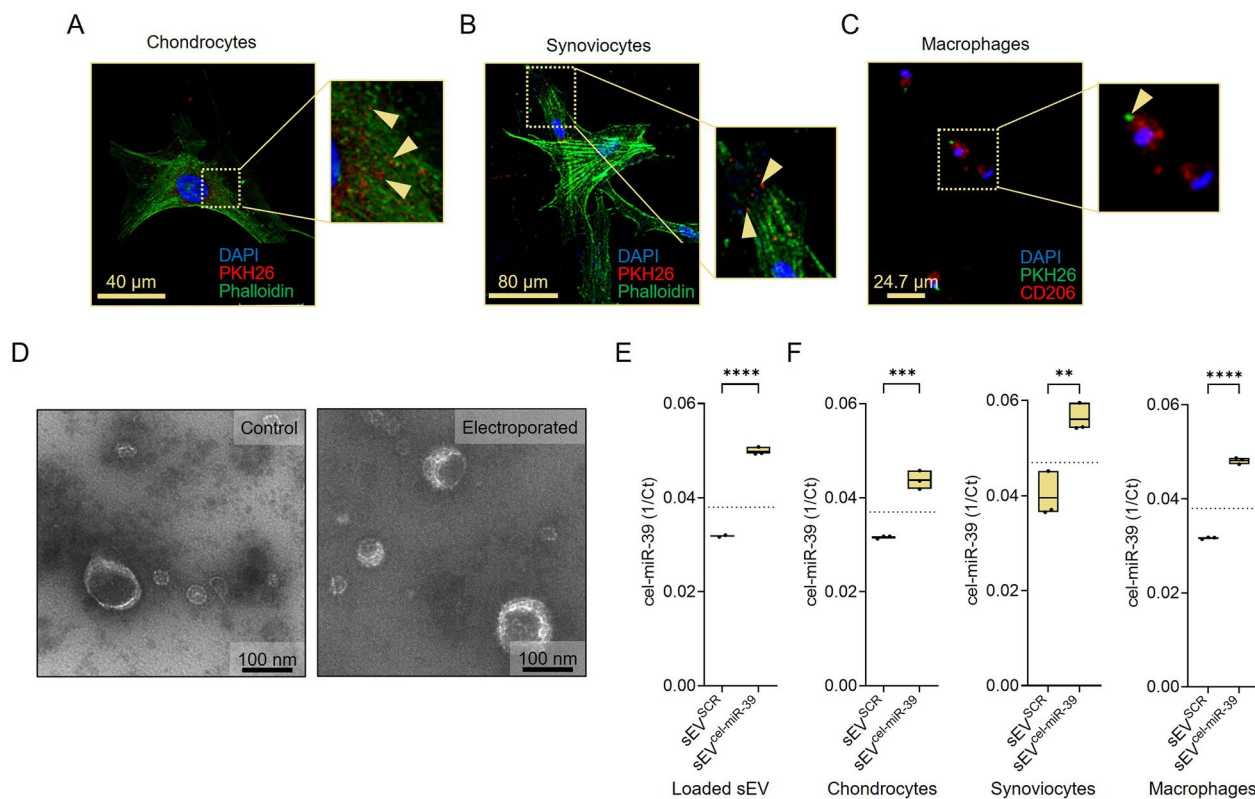


Fig. 2 sEV are internalized by key OA-related cell lineages and can be engineered to carry and deliver an external miRNA. PKH26-stained sEV internalization was evaluated after 24 h of incubation by confocal microscopy in: **A** huOAC, **B** synoviocytes and **C** hmMØs (DAPI = nucleus; Phalloidin = actin filaments; CD206 = macrophage surface protein). **D** TEM micrographs of sEV showing classical “cup-shape” morphology in control (left) and electroporated (right) sEV. **E** A qPCR was performed to detect the presence of *C. elegans* miR-39 in engineered sEV and **F** in engineered sEV-treated huOAC (left), synoviocytes (middle) and hmMØs (right) loaded with scramble (SCR) miRNA or *C. elegans* miR-39 (cel-miR-39). A Shapiro-Wilk test was performed as data normality test; unpaired t-test was applied for statistical analyses. n = 1 for internalization assays; n = 3 for engineered sEV assays.

in our purified sEV. Interestingly, the number of reads obtained for each miRNA detected showed that only 13 miRNAs represented ~70% of the total reads processed for each batch of sEV analyzed (Fig. 1J), which confirmed the feasibility of obtaining sEV with a specific and reproducible miRNA signature. In the proteomic analysis of sEV, a total of 420 distinct proteins were identified among the samples (392 in sample sEV^{donor 1}, 386 in sample sEV^{donor 2}, and 252 in sample sEV^{donor 3}) (Table S2), of which 236 proteins were shared between the three sEV samples (Fig. 1K). Of these proteins, 70 corresponded to proteins expected to be found in sEV isolates (Supplementary Fig. 6) [79, 87], confirming the EV and exosome nature of our UC-MSC-derived isolates. Taken together, these results suggest that despite variations in miRNA and protein compositions between sEV samples, a core set of miRNAs and proteins that are consistently present in UC-MSC-derived sEV exists. This implies a high standardization and reproducibility level in manufacturing, emphasizing the potential of producing sEV

with specific molecular signatures suitable for therapeutic applications.

UC-MSC-sEV internalization by key OA-related cell lineages promote an anti-inflammatory microenvironment and displays chondroprotective protection in vitro
UC-MSC-sEV internalization and cargo delivery in the OA joint microenvironment cells

In huOAC, flow cytometry analysis data showed progressive uptake and accumulation of sEV over a 24 h time (Supplementary Figs. 7A and B), confirming its intracellular location through confocal microscopy (Fig. 2A). Similarly, internalization of sEV was also observed in synoviocytes and macrophages (Fig. 2B and C, respectively). To confirm the delivery of sEV cargo, a proof-of-concept experiment using engineered sEV loaded with a synthetic miRNA (cel-39) derived from *Caenorhabditis elegans* was performed on chondrocytes, synoviocytes and macrophages. Characterization of the engineered sEV demonstrated that the loading protocol via electroporation

maintained vesicle size, quantity, integrity, and identity (Supplementary Fig. 8) and morphology (Fig. 2D). qRT-PCR analysis confirmed the successful loading of sEV with exogenous cel-miRNA-39 (Fig. 2E). Incubation of engineered sEV with chondrocytes, synoviocytes and macrophages revealed effective transfer of cel-miRNA-39 via direct internalization (Fig. 2F). Altogether, these results confirm that sEV can be taken up by various cell types present within the joint microenvironment and can deliver their molecular cargo to recipient cells. This underscores the potential therapeutic impact of targeted content delivery.

UC-MSC-sEV effect on monocyte-derived macrophage polarization

To investigate whether sEV-based treatment acts as a specific stimulus to hmMØs to predominantly adopt an M2-like phenotype (anti-inflammatory state), a hmMØs polarization assay was established and analyzed by flow cytometry and ELISA (Fig. 3A). As shown in Fig. 3B, sEV treatment decreases the expression of HLA-DR (fold change of 0.56 ± 0.13 respect to control) and CD86 (fold change of 0.82 ± 0.28 respect to control) and increases the expression of CD206 (fold change of 1.55 ± 0.54 respect to control) and CD163 (fold change of 1.25 ± 0.18 respect to control), suggesting the acquisition of an anti-inflammatory M2-like state. Due to M2-like macrophages exhibit significant phenotypic heterogeneity and can be subdivided into various subtypes: M2a, M2b, M2c, and M2d, each expressing specific markers, exhibiting unique cytokine profile, and performing varied function [72], a comprehensive study was conducted to assess diverse pro- and anti-inflammatory secreted cytokines. Figure 3C shows that the treatment with UC-MSC-sEV stimulate the secretion of IL-10 (control = 81.33 ± 20.42 pg/mL; sEV = 4149 ± 1561 pg/mL), VEGF (control = undetectable; sEV = 277 ± 114 pg/mL), IL-6 (control = 143.0 ± 243.2 pg/mL; sEV = 2250 ± 93.89 pg/mL), and TNF- α

(control = undetectable; sEV = 471.0 ± 177.6 pg/mL). An increasing trend was also observed for IL-1 β (control = 6.59 ± 11.43 pg/mL; sEV = 108.0 ± 69.32 pg/mL). This ambivalent secretory profile of both pro- and anti-inflammatory cytokines, along with the expression of CD86, suggests an increment of the polarization to an M2b-like subset [85]. Interestingly, this biological effect was consistent across various monocyte donors and sEV batches (Supplementary Fig. 9). Altogether, the data obtained demonstrate that UC-MSC-sEV treatment triggers an anti-inflammatory state in hmMØs, presenting the potential to contribute to the repair of damaged articular cartilage.

Chondroprotective activity of UC-MSC-sEV against oxidative stress

To study the chondroprotective activity of UC-MSC-sEV against oxidative stress, huOAC cells exposed to menadione—an agent known to induce cell death via ROS-dependent mechanisms [45]—were treated with UC-MSC-sEV (Fig. 3E). As shown in Figs. 3F and G, while menadione induced cell death in $80.61 \pm 11.47\%$ of cells, treatment with sEV mitigated this effect, diminishing cell death to $57.21 \pm 18.69\%$, demonstrating the chondroprotective activity of sEV against oxidative stress-induced cellular damage and their potential to mitigate OA progression.

Cytotoxicity profile of UC-MSC-sEV-based treatment

To investigate the safety of the sEV-based treatment in vitro, cytotoxicity based on the measurement of the cytoplasmic enzyme LDH was performed in huOAC cells after treatment with UC-MSC-sEV (Fig. 3H). LDH detection in the SN indicates plasma membrane damage, a characteristic of cells undergoing apoptosis, necrosis, and other forms of cellular damage [38]. The LDH release-based assay showed that sEV treatment did not elicit any alterations in LDH release into the

(See figure on next page.)

Fig. 3 sEV drives macrophage polarization and exerts chondroprotective activity against oxidative stress. **A** Schematic view of the established hmMØs polarization assay. **B** Representative plots of CD86/HLA-DR (M1, pro-inflammatory markers) and CD206/CD163 (M2, anti-inflammatory markers) obtained by flow cytometry analysis of control (untreated) and sEV-treated hmMØs are shown, followed by a graph summarizing the fold change of MeFI obtained for CD86, HLA-DR, CD206 and CD163 (control vs sEV treated). **C** Macrophage's cytokine production and secretion was determined by ELISA for IL-10, VEGF, IL-6, TNF- α and IL-1 β , respectively. **E** A menadione-induced cytotoxicity assay was performed to evaluate the chondroprotective activity of sEV by PI/Annexin V stain and flow cytometry. **F** Representative plots showing PI/Annexin V stain in huOAC as follows: no treatment control (top), menadione-treated (middle) and menadione + sEV treated (bottom). **G** Graphs depicting the percentage of live cells (left) and apoptotic/dead cells (right). **H** A LDH release-based cytotoxicity assay of sEV in huOAC was established. **I** LDH release determination in: (1) Triton X-100 treated huOAC (Control^{positive}), (2) untreated huOAC (Control^{negative}), (3) sEV-treated huOAC, dose I (100×10^6 sEV/well) and (4) sEV-treated huOAC, dose II (400×10^6 sEV/well). hmMØs polarization assay: $n = 5$ for flow cytometry and $n = 3$ for ELISA, a Shapiro-Wilk test was performed as data normality test followed by unpaired t-test; a.u. = arbitrary units; floating bars = min to max, solid line = mean. Menadione-induced cytotoxicity: $n =$ at least 6, a Shapiro-Wilk test was performed as data normality test followed by one way ANOVA with Tukey multiple comparisons test; floating bars = min to max, solid line = mean. LDH- based cytotoxicity: $n = 4$, Kruskal-Wallis test (non parametric data) followed by Dunn's multiple comparisons post-test, bars = mean \pm standard deviation, $\alpha = 0.05$.

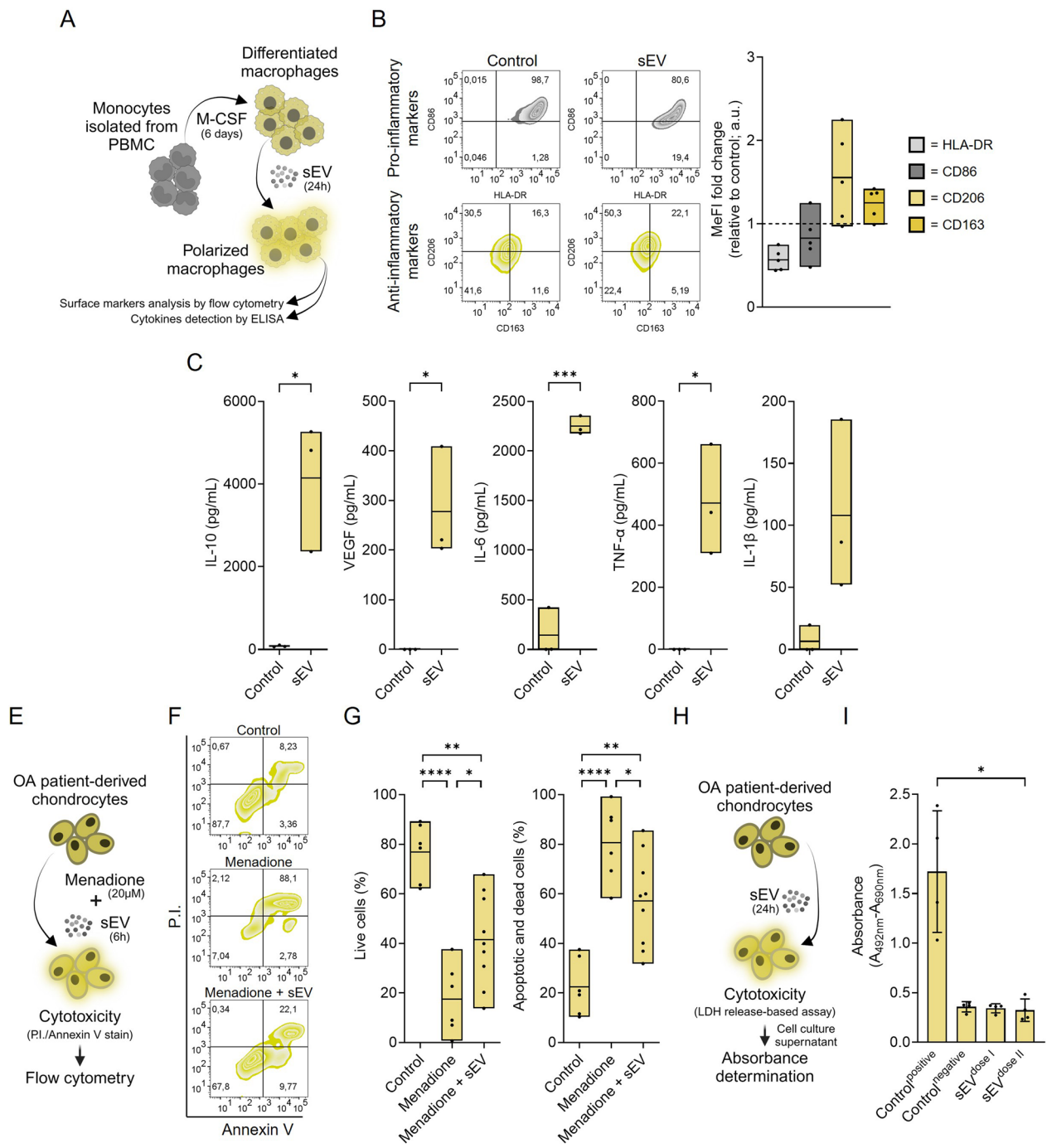


Fig. 3 (See legend on previous page.)

extracellular milieu of huOAC cells (Fig. 3I). This safety assessment indicated the absence of potential cytotoxic effects on primary cells forming hyaline cartilage,

demonstrating a favorable biocompatibility profile for the administration of sEV into the joint.

Molecular signature of UC-MSC-sEV unravel key players in macrophage-related processes and inflammation in OA

To elucidate the mechanism through which UC-MSC-sEV exert an anti-inflammatory effect on hmMØs, bioinformatics analysis was carried out to integrate data from miRNA profiles and proteomics to analyze interconnected biological networks. Among the ~1200 miRNAs identified in each sEV sample, close to 45% (corresponding to 516 miRNAs) exhibited sequence homology with entries in the online miRNET database [11]. Subsequently, by cross-referencing these 516 miRNAs with the HMDD database, a repository for experimentally supported human miRNA-disease associations [15], a subset of 16 common miRNAs was identified (Fig. 4A). The characterization of these 16 identified miRNAs revealed different expression patterns, highlighting the enriched levels of miR-320a, miR-107, miR-320c and miR-137 (Fig. 4B), due to the high number of targets (Table S3). Importantly, all 16 miRNAs were associated with processes implicated in OA (Table S4), emphasizing their potential relevance in this context. Gene ontology (GO) enrichment analyses of the targets of the selected miRNAs were conducted to identify the pathways related specifically to macrophages or inflammation that contribute to the anti-inflammatory mechanism. Biological processes, such as “macrophage differentiation”, “macrophages derived from cell differentiation”, “regulation of macrophage cytokine production”, and “macrophage cytokine production” were the terms with more genes associated with the pathway related to “macrophages” (Fig. 4C). In the GO category “inflammation”, the main terms identified were “inflammatory cell apoptotic process” and “inflammatory response to wounding” (Fig. 4D). The association between these miRNAs and their respective protein-coding gene targets within pathways is shown in Fig. 4E for macrophage-related processes and Fig. 4F for inflammation related processes, in which miRNA-107 and miRNA-320a stood out with the highest number of targets in these contexts. Of predicted target genes, highlight Signal transducer and activator of transcription 1 (STAT1), Matrix metalloproteinase 9 (MMP9), and Poly (ADP-Ribose) Polymerase 1 (PARP1), among others, since at least two miRNAs

shared them and, notably, were previously reported to be involved in the complex process of macrophage polarization (Table S5). Through the list of detected miRNAs, miRNA-222, miRNA-27a and miRNA-125a-5p were identified in all sEV batches. These miRNAs have been associated previously to play a crucial role into M2b-like polarization of macrophages [85]. In particular, miRNA-222 up-regulation polarizes monocytes to M2b-like macrophages [78], miRNA27-a is increased in M2b-like macrophages [25], and miRNA-125a-5p overexpression enhances M2b polarization [5]. This underscores their potential influence on key processes associated with macrophages and inflammation, suggesting a crucial role in the molecular landscape of OA. The full dataset is presented in Table S6.

Regarding the proteins identified in the sEV cargo, the GO analysis revealed significant enrichment in “macrophage migration,” “regulation of macrophage migration,” and “inflammatory response” in the biological process category. Notably, CD81, Apolipoprotein B (APOB), Integrin alpha V (ITGAV), and Integrin-β3 (ITGB3) were highly enriched in the macrophage-related processes (Fig. 4G). In addition, complement component 3 (C3), CD81, Serpin family E member (SERPINE1), and alpha-2-macroglobulin (A2M) were implicated in inflammation (Fig. 4H). Interestingly, SERPINE1 and A2M have been reported to be involved in binding pro-inflammatory molecules, promoting the M2-like phenotype, and attenuating cartilage degeneration and bone resorption in preclinical OA models via distinct signaling pathways [37, 54, 9983,]. These findings underscore the potential significance of these molecules in macrophage-related and inflammatory processes and offer valuable insights into their roles within the intricate molecular network associated with OA. The complete dataset is presented in Table S7.

In order to confirm the *in silico* predictions related to the role of sEV’s miRNA and protein cargo in regulating macrophage polarization and inflammation, RT-qPCR analysis was conducted to measure the transcript levels for Signal Transducer and Activator of Transcription 1 (STAT1) and Peroxisome Proliferator Activated Receptor Gamma (PPARγ) in hmMØs treated with sEV for 24 h.

(See figure on next page.)

Fig. 4 The deciphered molecular signature of sEV provides insights of their inflammation-related bioactivity *in silico*. **A** Venn diagram of sEV-miRNAs identified in our study, miRNet, and HDMM databases. **B** Enrichment patterns of the 16 common miRNAs in the analyzed samples. Subsequently, GO analysis of the identified proteins was performed, highlighting several biological processes and the number of putative target genes related to macrophage **C** and inflammation processes **D**. **E** Circular plot showing the association between identified sEV-miRNAs and their target genes within GO categories associated with “macrophage” **E** and “inflammatory” **F**, respectively. **G** GO category enrichment analysis specifically linked to the “macrophage” GO term, while **H** focuses on enrichment in the “inflammatory” GO term. **I** RT-qPCR validation of *in silico* predicted target gene *STAT1* in macrophages 24 h after sEV treatment and in M1 phenotype macrophages (left) and a schematic representation of the potential effect of sEV’s miRNA/protein cargo on macrophages phenotype through *STAT1* inhibitor (right)

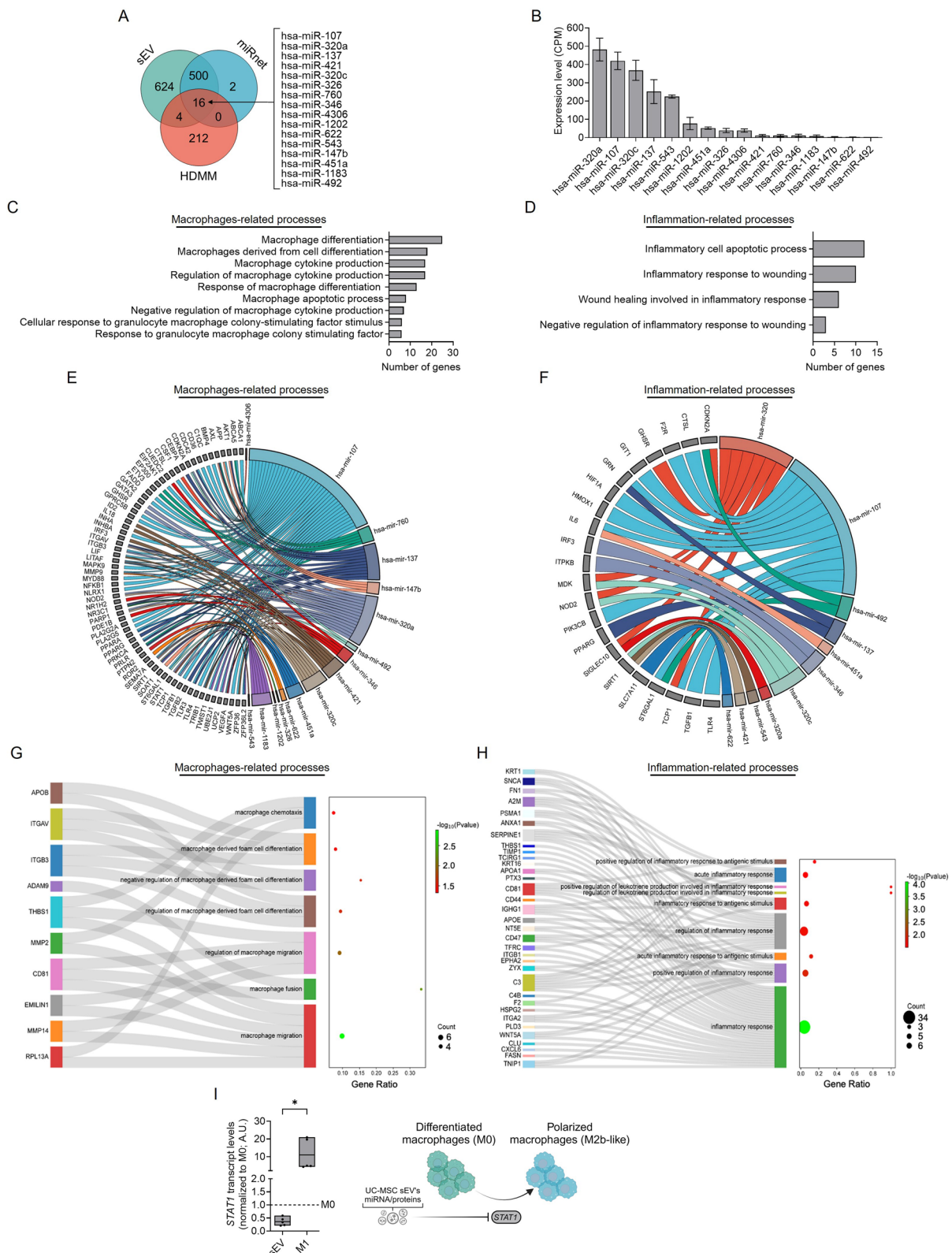


Fig. 4 (See legend on previous page.)

The results showed a decrease in *STAT1* transcript levels (Fig. 4I, left), supporting the modulatory effect of sEV on macrophage polarization. A decrease was also observed in *PPAR γ* transcript levels (Supplementary Fig. 10). Control macrophages treated with IFN γ /LPS (M1 phenotype) exhibited an expected increase in *STAT1* transcript levels [34] and a decrease in *PPAR γ* [93]. These findings confirm the capacity of sEV to shift macrophage profiles towards an anti-inflammatory phenotype. A summary schematic is presented (Fig. 4I, right).

UC-MSC-sEV exhibits an anti-osteoarthritic and anti-inflammatory effect in a collagenase in vivo model of OA

Therapeutic efficacy of UC-MSC-sEV treatment: μ CT and histologic analysis

On days 7 and 14 post OA induction, 2×10^8 particles were injected via IA (Fig. 5A). This concentration was established considering the highest number of particles attainable within a 5 μ L solution, corresponding to the maximum volume feasible for administration into a mouse knee joint [36, 74]. At 42 days post-OA induction, the mouse articular cartilage was subjected to histomorphometric and histopathological studies. Representative images obtained by μ CT are shown in Figs. 5B and D to assess the bone architecture of the joint. μ CT involves recording 2D X-ray images from various viewing angles around the freely rotating sample, which is followed by a 3D reconstruction generated by computer algorithms [62]. The 2D parameter corresponded to bone mineral density (BMD), which was employed to quantify the mineral total mass normalized by the volume of the analyzed zone, providing an estimate of bone integrity [26, 52]. μ CT analysis revealed decreased BMD in the lateral femur (0.001977 ± 0.0002000) as well as in the medial and lateral tibia (0.002362 ± 0.0003302 and 0.001915 ± 0.0002477 , respectively) joint areas of animals treated with sEV compared to the vehicle-treated group (0.002370 ± 0.0003670 , 0.002858 ± 0.0004405 , and 0.002214 ± 0.0003149 , respectively), with values approaching those of the sham group (0.001929 ± 0.0005558 , 0.002015 ± 0.0007867 and 0.001645 ± 0.0004973 , respectively) (Fig. 5C). Regarding the 3D parameters, the bone surface-to-volume ratio (BS/

BV) was assessed, a value that indicates the ratio between the surface area and volume of the region segmented as bone, providing a measure of the number of bone-lining cells covering a given volume of bone in the sample [52, 61]. The BS/BV analysis exhibited a drastic reduction in sEV-treated animals in all joint areas analyzed (medial femur = 9.158 ± 1.777 , lateral femur = 9.755 ± 1.478 ; medial tibia = 8.309 ± 1.492 ; and lateral tibia 9.651 ± 1.136 with respect to vehicle-treated (medial femur = 11.82 ± 2.071 ; lateral femur = 12.22 ± 1.337 ; medial tibia = 10.56 ± 1.492 ; and lateral tibia = 13.04 ± 1.655 and sham groups (medial femur = 11.29 ± 4.373 ; lateral femur = 10.44 ± 3.224 ; medial tibia = 10.32 ± 3.325 ; lateral tibia = 11.26 ± 4.553 (Fig. 4E).

Histological analysis revealed signs of joint regeneration in animals treated with sEV. Figure 5F displays representative images of each experimental group, where the articular cartilage layer is observed in red owing to the staining process. Although animals with OA displayed architectural loss and cartilage degradation, these findings were absent in the sEV-treated group. These results indicate that sEV-based therapeutic shields cartilage and bone from degradation in the CIOA murine model. Histologically, the severity of cartilage damage and the affected surface area were evaluated using the Pritzker OARSI score, which considers the degree of degeneration and depth of damage [57]. The clinical score obtained showcased low values in the articular regions of the medial femur, lateral femur, medial tibia, and lateral tibia in sEV-treated animals (10.59 ± 3.062 , 9.094 ± 2.782 , 10.53 ± 5.786 , and 10.86 ± 4.924 , respectively), akin to those in the sham control groups (3.971 ± 2.440 , 4.059 ± 2.947 , 3.529 ± 1.875 , and 4.531 ± 2.101 , respectively), and lower than the values obtained in vehicle-treated mice (18.37 ± 10.50 , 19.97 ± 10.27 , 17.27 ± 12.60 , and 26.72 ± 3.256) (Fig. 5G). These results demonstrated that sEV-based therapy has regenerative and protective therapeutic potential for hyaline cartilage in a murine model of OA, which must be confirmed in patients.

Immunogenic studies

To assess the potential anti-inflammatory and immunomodulatory effects of sEV, we investigated the

(See figure on next page.)

Fig. 5 sEV reduces the severity of osteoarthritis and promotes regeneration in a murine model in vivo. **A** Schematic illustration of pre-clinical sEV IA administration in a CIOA mouse model in vivo. **B** BMD representative μ CT images are shown following three treatments: Sham, OA and OA + sEV; the color corresponds to the degree of mineralization: higher numbers (blueish) on the scale represent a higher local mineralization (more mineral per volume). **C** BMD measurements generated from μ CT. Four different knee joint zones were evaluated: medial femur, lateral femur, medial tibia and lateral tibia. **D** μ CT-derived knee joint coronal images of sham, OA and OA + sEV-treated knee. **E** BS/BV index obtained from μ CT analyses in four different knee joint zones. **F** Histological verification of cartilage condition by Safranin O/Fast green stain. **G** OA histological scores obtained in four different knee joint zones. Box and whiskers plot (solid lines = median), n = 12 mice (at least); non parametric data, Kruskal-Wallis test followed by Dunn's multiple comparisons post-test, $\alpha = 0.05$

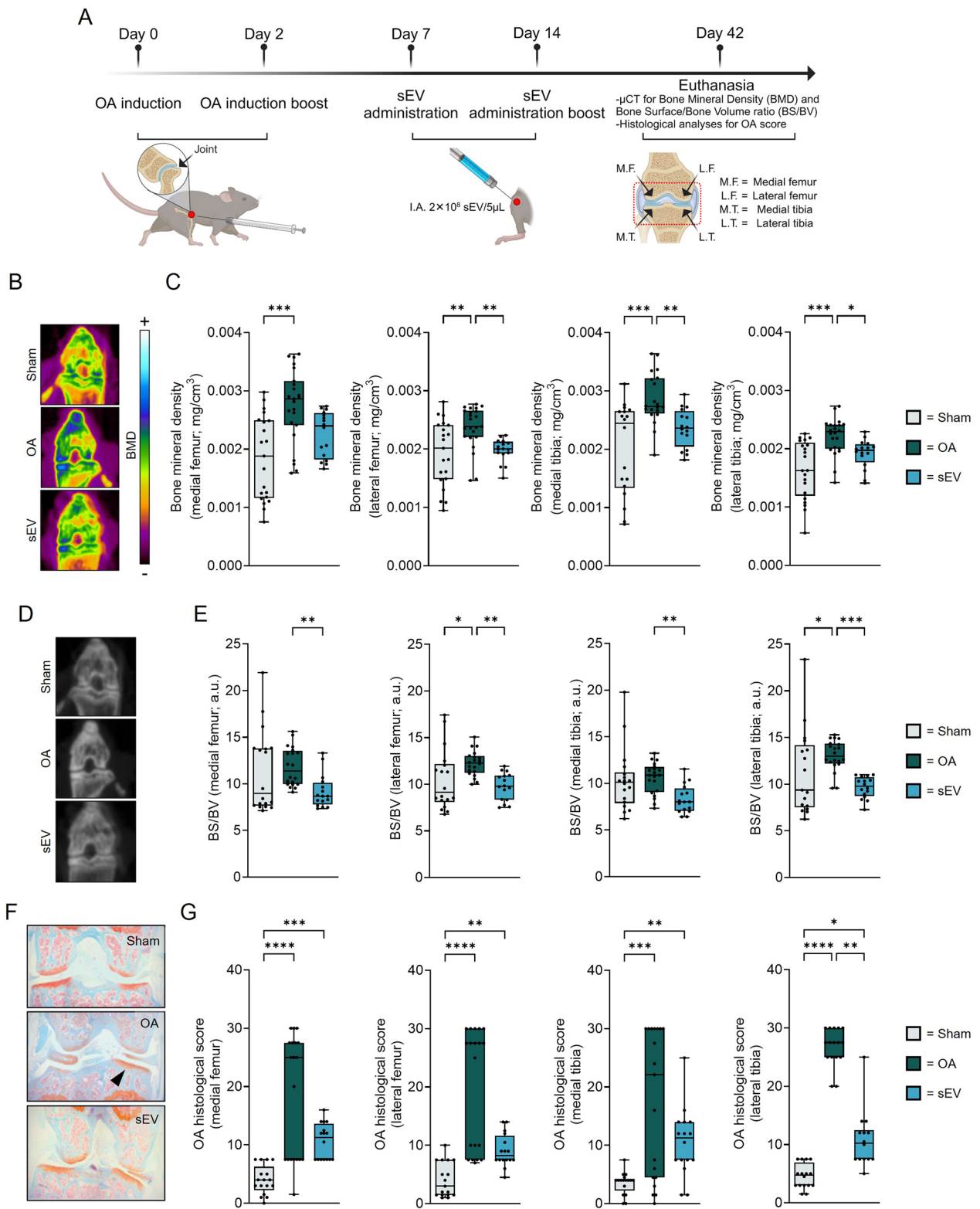


Fig. 5 (See legend on previous page.)

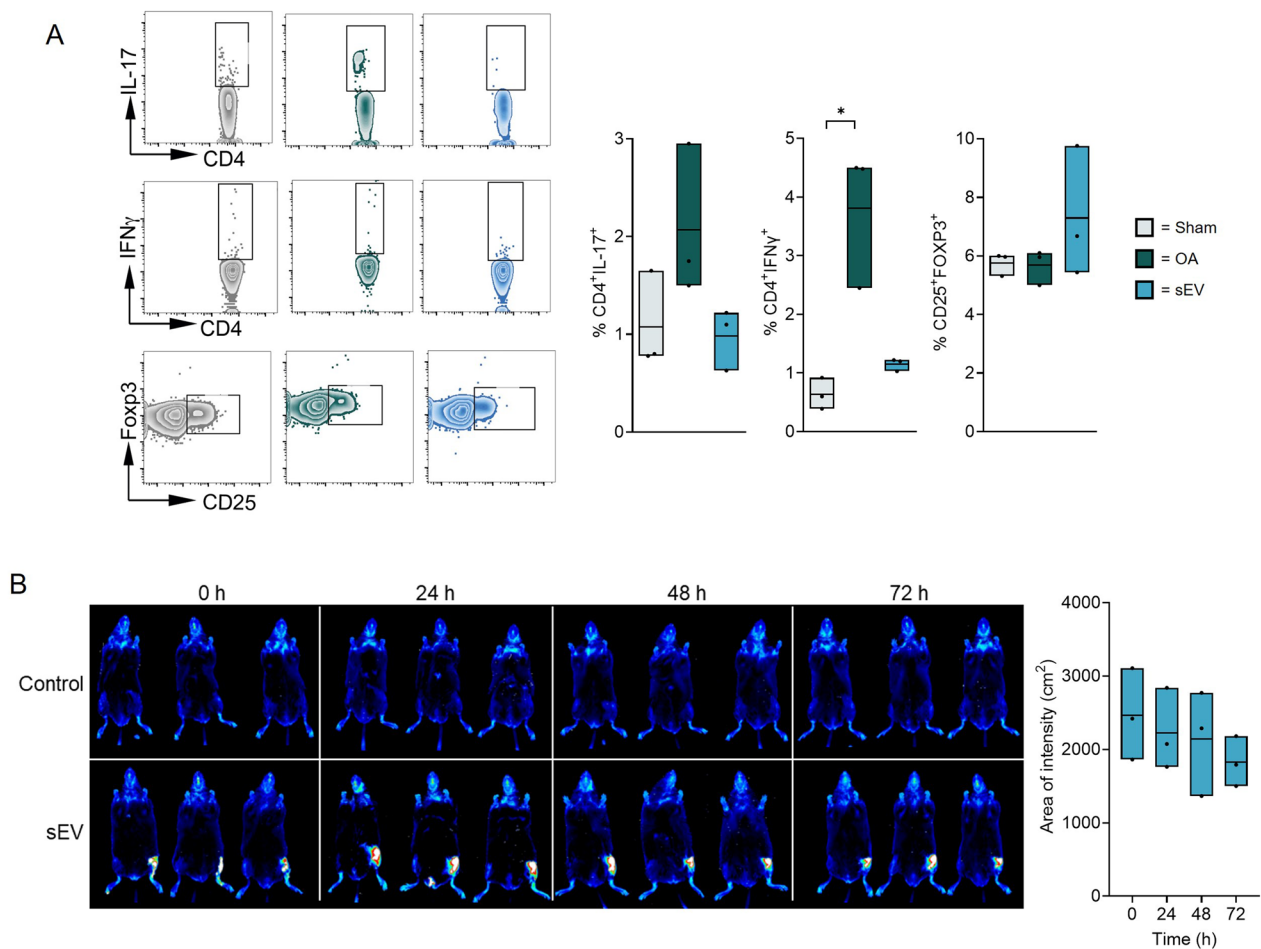


Fig. 6 sEV exerts immunosuppressive activity in vivo and are maintained within the knee joint space. **A** For murine *in vivo* immunogenicity assessment popliteal lymph nodes were isolated from sham, OA and sEV treated mice and T-CD4⁺ cell populations were determined by flow cytometry as follows: CD4⁺IL-17⁺ for proinflammatory cells; CD4⁺IFNγ⁺ for helper cells and CD25⁺FOXP3⁺ for Treg cells. Representative histograms for each subpopulation are shown (left) and subpopulations percentages are presented (right). **B** As biodistribution assay, DiR-stained sEV were administered by intra-articular injection in mice knees and monitored for 24, 48 and 72 h. Non parametric data; Kruskal-Wallis test, Dunn’s multiple comparisons post-test, $\alpha = 0.05$; n = 3 mice per group. Floating bars = min to max, solid line = mean

immune cell populations within the proximal popliteal lymph nodes following IA administration of sEV. After three days of IA sEV administration, the mice were humanely euthanized, and the drained lymph nodes were harvested for subsequent flow cytometry analysis. Our findings revealed that IA administration of sEV tended to decrease the proportions of CD4⁺IL-17⁺ cells, predominantly composed of pro-inflammatory Th17 cells, and significantly inhibits the population of CD4⁺IFN-γ⁺ cells, predominantly characterized by pro-inflammatory Th1 cytokine-producing cells, as compared to the OA control by two-fold and three-fold, respectively. In the case of CD25⁺FOXP3⁺ cells (T-reg cells), sEV IA administration tended to increase their percentage by a quarter (Fig. 6A). This observation

suggests an immunosuppressive activity exhibited by sEV derived from UC-MSCs, which is consistent with the previously observed immunomodulatory effects in *in vitro* assays and predicted by *in silico* assays based on the miRNA and proteomic cargo of sEV.

UC-MSC-sEV biodistribution after IA injection

To investigate the biodistribution kinetics of the sEV-based product following IA injection in vivo, healthy mice were administered a single injection of therapeutic doses (2×10^8 particles/knee). *In vivo* scans conducted at 24, 48, and 72 h post-injection revealed the presence of DiR-stained sEV in the knee joint. As shown in Fig. 6B, the signal from DiR-stained sEV remained localized within the knees of the animals for up to 72 h. *Ex vivo*

organ analysis was performed to evaluate the possible migration of sEV from the joint to other organs of the mouse body without detecting any signal from the DiR-stained sEV in the examined organs (Supplementary Fig. 11). These data indicate the retention of sEV at the administration site without significant migration to other organs during the study period, implying a favorable safety profile for IA administration of sEV.

Product development of UC-MSC-sEV

Homologation studies of sEV formulation

To translate the preclinical product into a formulation suitable for clinical use, it was necessary to substitute the carrier solution utilized in the preclinical product (PBS) with a solution that adhered to the standards required for therapeutic administration, such as RL solution. The homologation study of the generated sEV-based products was performed according to the MISEV recommendations to characterize sEV and evaluate their potency in the hmMØs polarization assay. Details are given in Appendix 1 and Supplementary Fig. 12. The findings demonstrated that sEV suspended in RL showed similar results to those suspended in PBS in terms of size, concentration, morphology, integrity, identity, purity, and potency. This highlights the suitability of RL as a vehicle for sEV suspensions and suggests its potential clinical applicability.

Long-term stability studies

To evaluate the stability of the sEV-based product under relevant storage conditions, sEV batches produced and enriched at a reduced scale were stored at -80°C for periods of 5 and 24 months. The results indicated no notable differences in the size mode, concentration, and presence of identity markers after storage for 5 months (Supplementary Fig. 13). Regarding the long-term stability

testing, the NTA analysis revealed minimal change in particle size (from 149.5 ± 15.18 nm to 161.1 ± 5.773 nm) along with a decrease to one third of particle concentration (time 0 = $3.26 \times 10^{11} \pm 2.14 \times 10^{11}$ particles/mL; time 24 month = $1.17 \times 10^{11} \pm 4.63 \times 10^{10}$ particles/mL) (Fig. 7A). Concerning the expression of canonical markers in sEV, the MeFI values suggested that storage for 24 months did not induce alterations in tetraspanins expression (Fig. 7B), maintaining the previously observed hierarchy: CD63 > CD81 > CD9. The assessment of sEV potency 24 months post-storage was also tested using the hmMØs polarization assay. The therapeutic sEV-based product retained its potential to induce an anti-inflammatory phenotype in macrophages, exhibiting an M2b-like polarization effect. This significant finding was characterized by reduced expression changes of HLA-DR and CD86, along with increased expression of CD206 and CD163 (Fig. 7C) and an increase in IL-10 (control = 78.88 ± 0.00 pg/mL; sEV = 149.8 ± 97.19 pg/mL), IL-6 (control = 17.64 ± 0.00 pg/mL; sEV = 547.3 ± 777.2 pg/mL), and TNF- α (control = not detected; sEV = 11.54 ± 14.24 pg/mL) secretion (Fig. 7D). This biological effect was consistent across the different monocyte donors (Supplementary Fig. 14). These results demonstrate that even after 24 months of storage, the vesicles maintained their identity and functional characteristics linked to anti-inflammatory properties despite the reduction in particle concentration.

Short-term stability studies

To validate the suitable timeframe between thawing and administration of the sEV product, a short shelf-life study was carried out using the thawed sEV maintained in the temperature range of $2-8^{\circ}\text{C}$. This temperature range was investigated because of its optimal suitability for logistics, transportation, and storage of products

(See figure on next page.)

Fig. 7 sEV phenotype and activity is stable after prolonged storage and thawing. **A** Size mode and concentration evaluated by NTA of sEV resuspended in RL after 24 months of storage. **B** The presence of CD63, CD81 and CD9 was evaluated before and after 24 months of storage at -80°C by bead-based flow cytometry. Representative histograms followed by the fold change of MeFI of each marker relative to its respective isotype control are shown. **C** Macrophage polarization assay with sEV stored in RL after 24 months at -80°C ; representative plots of untreated (control) and sEV-treated macrophages are shown for pro-inflammatory markers (CD86/HLA-DR) and anti-inflammatory markers (CD163/CD206), followed by MeFI fold change of each marker, depicting the polarization towards an anti-inflammatory phenotype. **D** IL-10, IL-6 and TNF- α presence determination by ELISA in macrophage supernatants. Next, sEV stored in RL were thawed from -80°C and stored at $2-8^{\circ}\text{C}$ for 24 h. **E** sEV size mode and concentration was evaluated by NTA. **F** Presence of CD63, CD81 and CD9 in sEV was evaluated by bead-based flow cytometry. Representative histograms followed by the fold change of MeFI of each marker relative to its respective isotype control are shown. **G** hmMØs polarization assay with sEV stored in RL using three independent monocyte's donors for macrophage differentiation and polarization assay; representative plots of untreated (control) and sEV-treated macrophages are shown for pro-inflammatory markers (CD86/HLA-DR) and anti-inflammatory markers (CD163/CD206), followed by MeFI fold change of each marker, depicting the polarization towards an anti-inflammatory phenotype. **H** IL-10, VEGF, IL-6, TNF- α and IL-1 β presence determination by ELISA in macrophage supernatants. A Shapiro-Wilk test was performed as data normality test; unpaired t-test was applied for statistical analyses, $n = 4-5$ for storage at 24 months and $n = 3$ for stability after thawing; a.u. = arbitrary units. Floating bars = min to max, solid line = mean. Percentages in representative histograms refers to the bead population

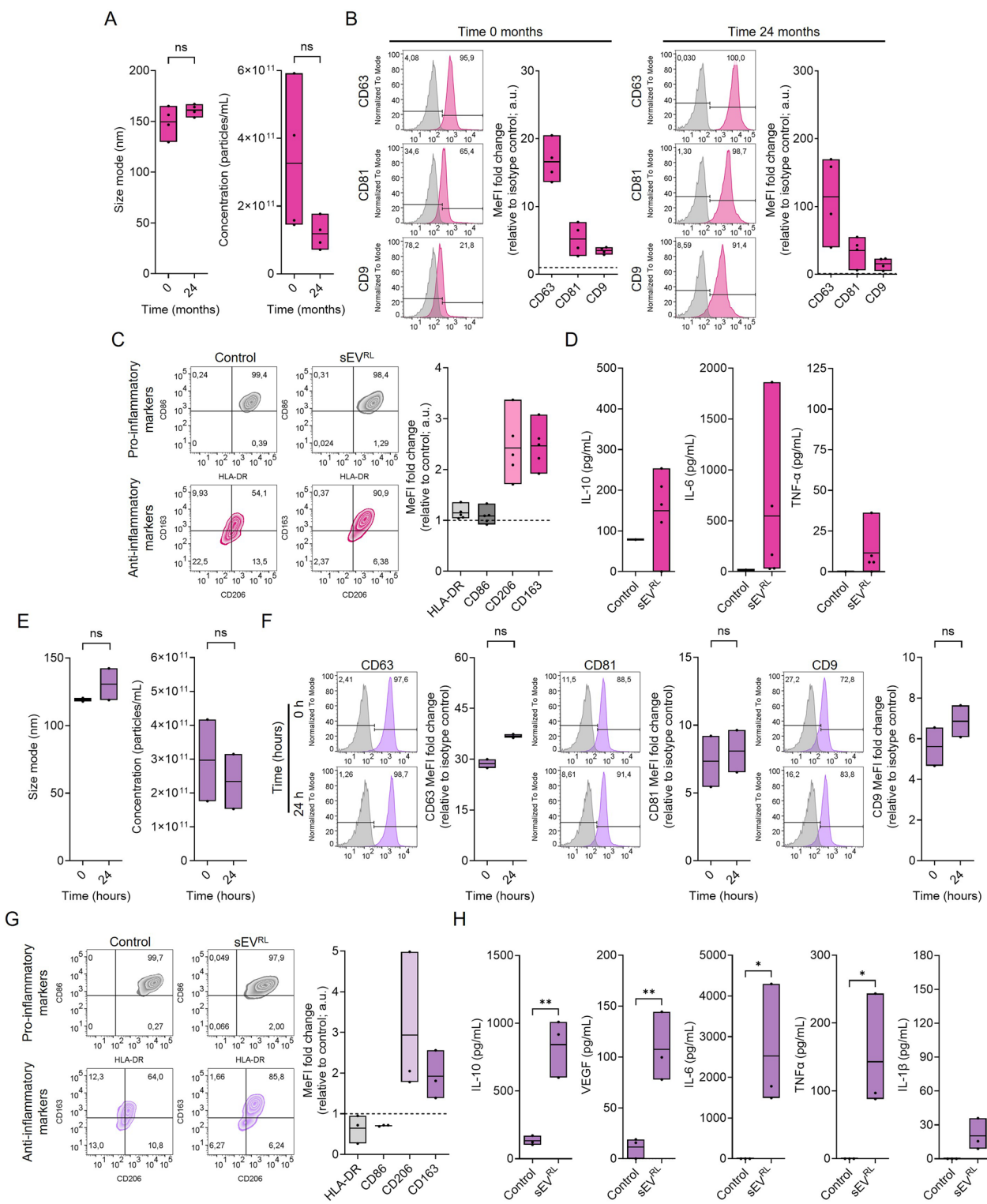


Fig. 7 (See legend on previous page.)

within facilities where this therapeutic approach can be applied. As shown in Fig. 7E, both the particle modal size and the concentration of the formulation

remained stable at 24 h (size: 130.6 ± 11.7 nm; concentration: $2.34 \times 10^{11} \pm 1.14 \times 10^{11}$) compared to the initial time point (size: 119.2 ± 1.2 nm; concentration:

$2.96 \times 10^{11} \pm 1.70 \times 10^{11}$). Regarding the identity markers, the MeFI values revealed that the expression of the tetraspanins remained consistent at 24 h (CD63 = 36.9 ± 0.5 ; CD81 = 8.1 ± 1.6 ; CD9 = 6.9 ± 0.8) compared to the basal time (CD63 = 28.7 ± 1.3 ; CD81 = 7.3 ± 1.9 ; CD9 = 5.6 ± 0.9) (Fig. 7F). Potency assays showed that 24 h storage does not alter the capacity of the sEV product to drive hmMØs towards the M2b state. Flow cytometry showed the increased expression of CD206 and CD163 along with reduced expression changes of HLA-DR and CD86, as shown in Fig. 7G. Likewise, cytokine quantification demonstrated an increased secretion compared to control macrophages of IL-10 (control = 132.4 ± 34.94 pg/mL; sEV = 842.2 ± 215.5 pg/mL), VEGF (control = 11.57 ± 10.15 pg/mL; sEV = 107.3 ± 33.97 pg/mL), IL-6 (control = not detected; sEV = $2,523 \pm 1,541$ pg/mL), TNF- α (control = not detected; sEV = 142.9 ± 87.24 pg/mL) and IL-1 β (control = not detected; sEV = 20.16 ± 14.10 pg/mL) (Fig. 7H). Collectively, these data show that thawed sEV therapeutics remain stable for 24 h at temperatures ranging from 2 °C to 8 °C. During this period, no significant alterations in size, concentration, specific protein markers, or potency were observed. Consequently, storing sEV within this temperature range could be an optimal storage condition.

Case report: first-in-human sEV administration in osteoarthritic knee

A 56 year-old woman with symptomatic knee OA was recruited for the IA injection of sEV. Owing to her professional occupation, she spent most of the day on her feet. Initial assessment revealed a pain-centric clinical presentation, with a limited gait range of 40 m and Kellgren-Lawrence stage II OA evident on radiography. She had no history of infiltration, arthroscopy, or surgery of the affected joint. Clinical examination indicated the absence of deformity, effusion, and preserved joint range, along with a positive patellar grinding test and negative Apley compression test. The body mass index was 30.2 kg/m^2 .

Patient-infiltrated therapy was subjected to strict quality controls at critical stages of the manufacturing process for its approval for clinical use, including its characterization by immunophenotyping for CD63, CD81, and CD9 markers. Syntenin-1, Flotillin-1 and Calnexin were not

detected by WB. Sterility was verified by automated aerobic/anaerobic blood culture testing, mycoplasma and endotoxin tests, and all tests were negative.

The patient's baseline visual analogue scale (VAS) score was 60 mm, and her Western Ontario and McMaster Universities Osteoarthritis (WOMAC) index was 79.6 (pain = 13, stiffness = 5, function = 61.6). After six months, the VAS and WOMAC indices were markedly reduced to 0 mm and 2 (pain = 0, stiffness = 0, function = 2), respectively. At 12 months, a sustained response was evident, with a VAS score of 0 mm and WOMAC index of 23 (pain = 3, stiffness = 2, function = 18) (Fig. 8A), allowing the patient to complete an unrestricted 200 m walk. Safety assessments revealed only transient post-injection pain, which was managed with acetaminophen and ibuprofen, and no joint effusion. No local or systemic symptoms or diseases were recorded during the 1 year follow-up. MRI images of the patients' knees at baseline and six months (Fig. 8B) were analyzed by Image Analysis Group (IAG; a third party based in London, UK). Following QC using IAG's proprietary technology and processes, the volumetric sequences SAG 3D SPAIR and SAG 3D WATSc were selected to study the progression of cartilage damage. Quantitative volumetry obtained via artificial segmentation of the femoral cartilage showed consistent hyaline cartilage volume pre- and post-treatment in both SAG 3D SPAIR and SAG 3D WATSc sequences, with no sign of degradation (Fig. 8C).

Clinical trial design

In phase I, three cohorts are planned with four subjects in each cohort receiving a three-fold escalating dose of $2 \times 10^9 \pm 0.5 \times 10^9$ total particles, $6 \times 10^9 \pm 0.5 \times 10^9$ total particles, or $2 \times 10^{10} \pm 0.5 \times 10^{10}$ total particles. These exploration doses will seek to determine the optimal dose to advance to phase II. Due to the characteristics of the sEV-based product and its manufacturing considerations, the exploration dose in the clinical case ($2 \times 10^{10} \pm 0.5 \times 10^{10}$ total particles) was established as the maximum tolerable dose feasible to investigate in the early-phase clinical trial. The medium and low doses correspond to a reduction of three-fold each, an escalated dose magnitude recommended by the FDA in its guidance for the design of early clinical trials using cellular products 17.

(See figure on next page.)

Fig. 8 First-in-human sEV administration over time and phase I clinical study design. **A** WOMAC index evolution during one-year post- sEV administration, divided in subscales: pain, stiffness and function. **B** Representative sagittal views of the first patient's right knee at baseline (left) and 6 months following sEV therapy treatment (right). Articular cartilage is indicated by arrows in lateral femur condyle and lateral tibia condyle. Images were analyzed by an external company using proprietary software. **C** Six month comparison of cartilage volumetry based on SPAIR and WATSc sequences obtained from third party's image analysis report. a.u. = arbitrary units. **D** Clinical phase I study design outline

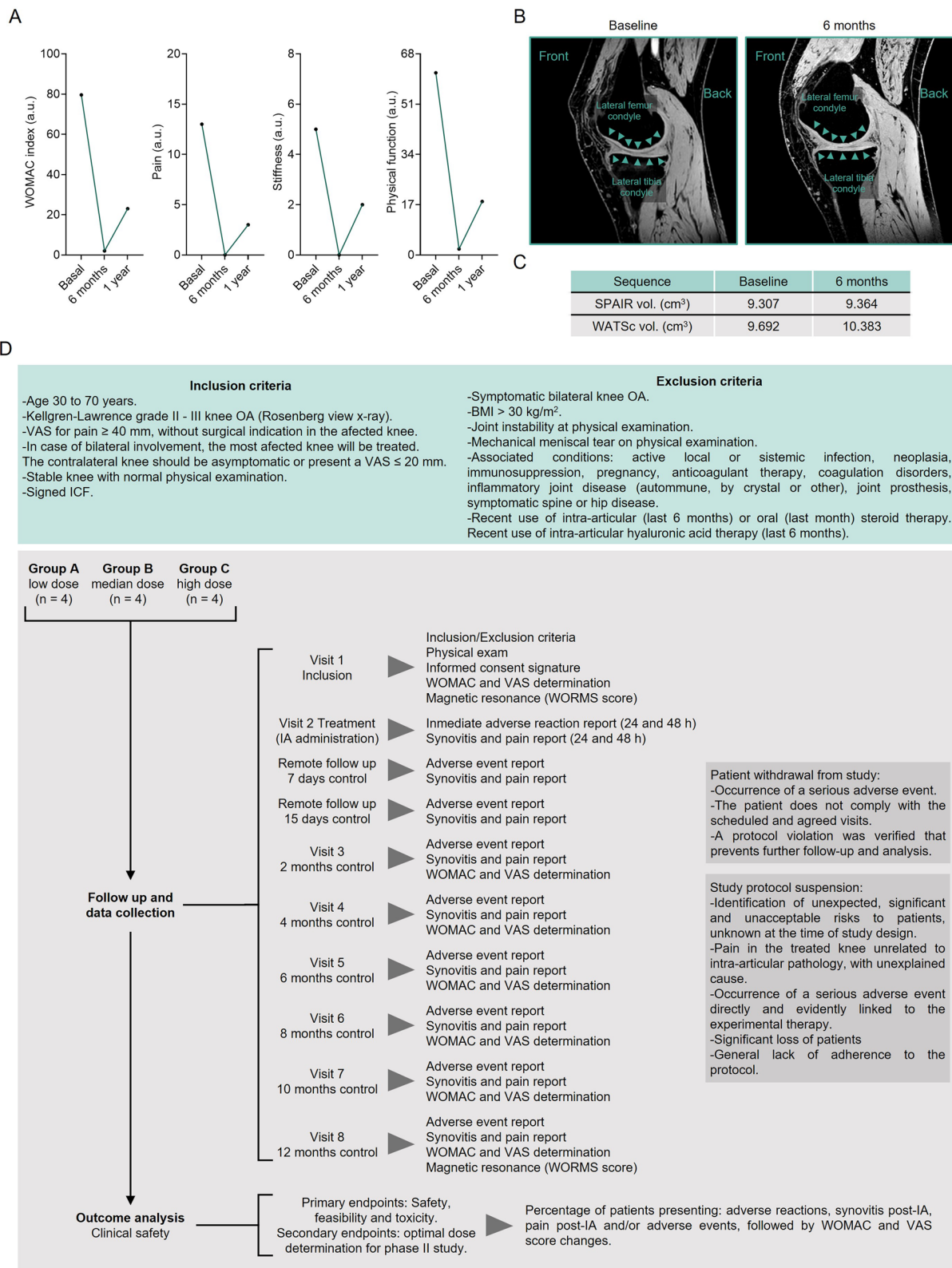


Fig. 8 (See legend on previous page.)

For the phase I, controlled, prospective, non-comparative clinical trial using a defined dose-escalation protocol of UC-MSCs-sEV for the treatment of knee OA, the incidence of both serious and non-serious adverse events directly attributed to- or resulting from the sEV infusion will be reported. This evaluation will extend from the early post-infusion period through 12 months of follow-up. The analysis of the primary safety endpoint will focus on the characterization of the proportion of adverse events in each treatment arm, while the secondary endpoint will be used for the design of the phase II trials. The analysis of the change in the WOMAC and VAS scores will allow us to evaluate the effectiveness of the product based on sEV in a small sample size. Analysis of the frequency of adverse events along with overall assessment of potential efficacy using clinical endpoints will allow us to determine safety and whether to proceed with a phase II trial. The study design flow is summarized in Fig. 8D.

Discussion

The clinical use of cell-derived biologics such as sEV encompasses different modalities, and their manufacturing processes may be vastly different from those of other therapeutics. Although identifying appropriate preclinical *in vivo* models to study the potential of sEV-based therapeutics can be challenging, the findings of this study, based on a well-established CIOA animal model, underscore the potential of UC-MSCs-derived sEV as a novel therapeutic avenue to address the complexities of OA. The success of the early development of novel therapeutics is heavily dependent on robust findings and complete preclinical data focusing not only on function, safety, and efficacy, but also on manufacturing, quality control, scaling, stability, and storage cues. Hence, issues related to pharmaceutical categorization are essential, and the regulatory aspects of the manufacturing and application of new therapeutics must be vigorously implemented [40]. A unified framework from early phase development to the commercialization of sEV-based drug products is still in progress. Nonetheless, we provide substantial advances in establishing a robust framework, beginning with the development of a sEV-based therapy, demonstrating consistent production, reproducible batches, and confirming the safety of clinical-grade products via initial human trials. The outcomes of our preclinical studies are consistent with those of prior research highlighting the regenerative and anti-inflammatory properties of MSC-sEV in mitigating joint degeneration, especially in the context of osteoarthritis [8, 13, 60, 70].

In our previous controlled randomized phase I/II trials, we described the safety and anti-inflammatory effect of IA injection of UC-derived MSC, the parental cells used to produce sEV. We also identified optimal dose

and number of injections required to achieve clinical efficacy in patients with OA [47, 48]. The demonstration of the safety and clinical efficacy of the parental cells is relevant for de-risking the use of UC-MSCs-derived sEV, but it cannot be fully extrapolated to the sEV product, and similar studies need to be performed. In this study, detailed characterization of UC-MSCs-derived sEV under non-cGMP conditions underscores their potential as a therapeutic option for OA. The manufacturing protocol follows a designed workflow adhering to the stringent guidelines of the USA CFR FDA Title 21, Part 211: Current Good Manufacturing Practice for Finished Pharmaceuticals (§211.1–211.208), from tissue procurement to final product packaging, validating the identity and purity, and ensuring reproducible production of the isolated UC-MSCs-sEV. Comprehensive analyses, including morphology, size, and protein marker assessments, confirmed the small extracellular vesicle classification [87]. Notably, a specific expression pattern of transmembrane tetraspanins was identified in all the sEV batches, with a consistent hierarchy of CD63 > CD81 > CD9. Syntenin-1 expression in sEV products has also been detected, providing evidence to support an endosomal biogenesis pathway for these extracellular vesicles [4]. The presence of MSC surface antigens CD90 and CD44 [16], was confirmed in the sEV products, indicating their MSC cellular origin [89]. The reduced MHC class I expression and absence of MHC class II in sEV products suggests a potential immune privilege that limits recognition by cytotoxic T cells and minimizes immune response risks [66, 71]. This characteristic, which is expected due to the parental cell origin [7], enhances the safety profile of allogeneic sEV-based therapies. The molecular cargo profile revealed a consistent shared repertoire of miRNAs and proteins, indicating the degree of standardization of the manufacturing process. Despite the inherent variability between samples, identification of a core molecular signature suggests the practicality of obtaining sEV with reproducible and specific compositions. The established reproducibility and consistency of the molecular cargo of sEV are clear advances that promote confidence in translating preclinical developments into clinically relevant therapeutic interventions. While some studies have suggested that EV-borne miRNAs do not act as effectors of cell-to-cell communication [1], future research should delve into elucidating the specific contribution of this core molecular signature to the observed therapeutic effects in OA, paving the way for a better understanding of the treatment's MoA.

Although the therapeutic impact of sEV may not depend exclusively on the internalization and transfer of their molecular cargo, evidence in literature underlines the pivotal role of these mechanisms in achieving

therapeutic actions [49]. In this study, the internalization of sEVs in key cells for the regulation of OA progression, such as chondrocytes, synoviocytes, and macrophages, was evaluated [29, 28, 73, 90]. The internalization assay confirmed the intracellular presence of sEV in these cells, confirming their potential as acceptors for the therapeutic effects mediated by sEV. A proof-of-concept experiment demonstrated a miRNA cargo shuttle in chondrocytes, synoviocytes and macrophages, emphasizing the specificity and potential therapeutic impact of sEV-mediated content delivery within diverse cell types constituting the OA joint microenvironment.

In OA pathology, inflammation and oxidative stress are closely integrated during disease progression, with elevated inflammatory mediators contributing to joint tissue abnormalities [46]. Local inflammatory responses, spearheaded by resident macrophages with a predominant pro-inflammatory phenotype [35], increase oxidative stress and accumulate ROS [46]. This alters cellular homeostasis in the joint, affecting cartilage metabolism and the viability of its cellular components, while perpetuating the inflammatory cascade [58]. Regulating the cellular redox balance and reducing the prevalence of pro-inflammatory macrophages within the joint are pivotal considerations for mitigating the severity of OA, as previously described [41, 43, 82]. In this context, our *in vitro* data showed that sEV treatment triggered the polarization of naïve (M0) macrophages into an M2b-like phenotype by targeting critical transcription factors involved in macrophage polarization and protected hOAC from ROS-induced apoptosis. M2b macrophages, also known as regulatory macrophages, are characterized by the expression of CD86 and various pro-inflammatory cytokines, such as TNF α , IL-6, and IL-1 β , and elicit significant expression and secretion of the anti-inflammatory IL-10 cytokine [85]. Our findings suggest that the molecular mechanisms underlying this polarization may involve the modulation of STAT1. By downregulating STAT1 expression, sEV facilitate a shift towards a macrophage profile that supports resolution of inflammation and tissue repair, processes that are essential for protecting chondrocytes and maintaining joint homeostasis in OA. The acquisition of an M2b phenotype is crucial for resolving inflammation in the OA joint, since these cells significantly suppress the immune response, impede naïve macrophage polarization into an M1-like state, and resist repolarization into M1-like macrophages [10]. This would contribute to reducing extracellular inflammatory proteins and simultaneously protecting chondrocytes from ROS-induced apoptosis and establishing a healthy microenvironment. These findings are consistent with previously reported results for other experimental MSC-sEV therapies, where an anti-inflammatory effect

on macrophages was also observed [42, 9755]). At the clinical level, the M1/M2 macrophage ratio has been significantly associated with the Kellgren-Lawrence grading system in knee OA, indicating that it is a potential predictor of OA severity [43, 101]. The immunomodulatory effects on macrophage reprogramming shown here, might additionally, represent the MoA by which sEV can skew the inflammatory microenvironment towards a pro-chondrogenic status, leading directly to a decrease in pain and stiffness scales in patients. Investigating the potential of UC-MSC-sEV products to repolarize M1-like macrophages into the M2b-like state and validating their biological impact on synovial macrophages will be investigated in future studies.

By performing *in silico* analysis, we identified at the molecular level that miRNAs and proteins transported by sEV may be involved in orchestrating molecular events, particularly related macrophage-mediated inflammatory responses. Using various bioinformatic tools, the analysis revealed 16 miRNAs with distinct functionalities related to OA and immunological processes, as documented in several studies. miRNA-107 has been identified for its protective role against knee OA, which is characterized by the reduction of caspase-1 activity and the inhibition of IL-1 β [64]. Furthermore, circulating miRNA-320a has been linked to the promotion of an M2-like immunosuppressive phenotype, suggesting its possible involvement in the regulation of inflammation [21]. In addition, miRNA-222-3p, miRNA-27a and miRNA-125a-5p were detected in all sEV batches. These miRNAs have been associated to play a crucial role into M2b-like polarization of macrophages [85]. In line with these findings, we validated *STAT1* and *PPAR γ* as potential miRNA target genes in macrophages, which was also associated with an increase in IL-10 production in macrophages exposed to sEV. The above findings allow us to better understand the molecular mechanisms that may be modulated by UC-MSC-sEV and potentially intervene in the inflammatory processes associated with OA using sEV enriched in specific molecular components to further improve their impact on immunological processes.

The efficacy of UC-MSC-sEV treatment was demonstrated in the CIOA murine model, where μ CT analysis revealed reduced BMD and BS/BV in sEV-treated animals, indicating a protective effect on joint integrity. Notably, histological assessment showed signs of joint regeneration, confirming the role of sEV in protecting cartilage and bone from degradation. The Pritzker OARSI score also indicated the regenerative potential of sEV therapy for hyaline cartilage. Additionally, immune cell analysis revealed an anti-inflammatory effect, reducing the number of pro-inflammatory Th17 and Th1 cytokine-producing cells after sEV administration.

Previous studies using UC-MSC-sEV-based therapies reported outcomes similar to those observed in this study [102]. For example, the study conducted by Li et al. [42] indicates that UC-MSC-sEV can alleviate cartilage degradation in OA by delivering key proteins and modulating the PI3K-Akt signaling pathway through miRNAs, promoting M2-like macrophage polarization, and exhibiting potent immunomodulatory potential. Likewise, Zhou et al. [100] report that UC-MSC-sEV treatment inhibits the secretion of pro-inflammatory factors in macrophages, prevents cartilage extracellular matrix degradation, enhances chondrocyte proliferation and migration, and inhibits chondrocyte apoptosis.

With respect to the biodistribution studies, the data indicates that sEV remain localized in the joint space for at least 72 h. This result reinforces the safety profile for IA administration due to the absence of leakage of sEV to other organs. Coupled with the expression profile of MHC class I and II in sEV and the absence of cytotoxicity observed in huOAC after different treatment doses *in vitro*, these results collectively confirmed the safety profile of the therapy in non-clinical safety studies. The choice of local delivery through IA administration provides an advantage by ensuring higher concentrations of sEV to the site of injury and increasing their uptake by target cells, particularly those within the knee joint space, while limiting off-target effects and the necessity of high and repetitive dosing.

After establishing the efficacy and safety profile in pre-clinical settings, the development of the UC-MSC-sEV product began with GMP homologation and validation to meet regulatory requirements and ensure the safety and quality of treatment. The product demonstrated consistency in size, concentration, and identity after modification of its formulation (RL as the vehicle). Notably, the sEV-based product retained its potency, defined as its ability to induce an anti-inflammatory state in naïve macrophages. After rigorous evaluation of its stability, the functionality of the product during long-term storage and within a defined shelf life was evident, further validating the potential of UC-MSC-sEV as a viable and robust therapeutic option for clinical translation.

The safety profile and promising impact of sEV-based therapy was evident in a 56 year-old woman with knee OA which highlights the potential therapeutic activity of sEV for OA treatment. Following IA administration, the patient showed notable and long-lasting improvement in pain and disability. Clinical assessments, including VAS and WOMAC index scores, showed substantial improvements at 6 months and persisted at the 12 month follow-up. The patient's unrestricted completion of a 200 m walk further denotes the potential therapeutic efficacy of sEV in managing knee OA symptoms. Safety analysis

revealed only transient pain post-injection, well managed with medication, with no recorded adverse events during the 1 year follow-up, indicating a favorable safety profile. Imaging assessments using a third party's proprietary image analysis software indicated the absence of degenerative cartilage damage progression post-sEV treatment, suggesting that sEV intervention did not harm the joint structure. Moreover, the consistent values of femoral cartilage volume shown by the UK-based imaging company suggested that sEV therapy "may halt cartilage reduction". The increase of WOMAC index scores at one year is expected as sequential dosing might be needed. The frequency and dose responses will be addressed in sequentially planned clinical phases following the analysis of findings from the upcoming phase I clinical trial.

The design of the phase I clinical trial was based on a wealth of knowledge, integrating insights from diverse sources. Our prior clinical experience with OA therapy using UC-MSCs [47, 48] provided a foundational understanding. This experience, coupled with considerations of joint size and anatomy in mice and humans, informed by preclinical dosage data obtained from the murine OA model were pivotal for the dosing approach. Real world evidence and insights gleaned from Dr. Rohde's group regarding the local intracochlear clinical application of sEV [86], was also taken into consideration in defining the dose-escalation protocol. The manufacturing feasibility of the sEV-based product were also examined, further influencing the design of the protocol. This was particularly pertinent as the concentration of sEV that can be locally administered in the knee joint is strongly determined by the maximum volume of product that can be delivered into this joint (1–3 mL maximum volume according to information obtained directly from surveyed orthopedic surgeons). The manufacturing capacity also influenced the trial design and size of the cohorts, as cautioned in the FDA guidance "Considerations for the design of early-phase clinical trials of cellular and gene therapy products" [17]. This collective knowledge guided the development of the submitted dose-escalation protocol.

Given the influence of manufacturing processes on the clinical application of sEV, the impact of manufacturing processes on the clinical application of sEV cannot be overstated. As we advance safety and clinical efficacy studies of sEV-based therapies, there is an urgent imperative to design, implement, standardize, and validate new manufacturing protocols on larger scales. These protocols must enable the production of higher treatment doses, facilitating diverse therapeutic regimens for patients who stand to benefit from these innovative advanced therapies.

Conclusions

This research demonstrates a pioneering clinical treatment employing UC-MSC-derived sEV for the treatment of OA, providing preclinical evidence supporting the efficacy and safety of this therapeutic modality, and culminating in safe translation to the clinic. A registered phase I safety trial is currently underway in which single doses of UC-MSC-sEV are administered by intra-articular injection in 12 patients with moderate knee OA (NCT no. 06431152; title: “Administration of sEV derived from UC-MSC in patients with osteoarthritis of the knee: safety determination in a pilot dose-escalation study”) with a 12 month follow-up [80].

This study establishes a standardized manufacturing protocol and a feasible workflow for clinical grade sEV. It demonstrates initial safety in a first-in-human IA administration. Additionally, by establishing a proof-of-concept for upcoming studies into cutting-edge therapy modalities for the management of OA, it fills the gap between preclinical promise and initial clinical application. Lastly, the developments discussed here provide a framework for developing regenerative medicine treatments for degenerative joint diseases.

Supplementary Information

The online version contains supplementary material available at <https://doi.org/10.1186/s12951-024-03088-x>.

Supplementary Material 1.
Supplementary Material 2.
Supplementary Material 3.
Supplementary Material 4.
Supplementary Material 5.
Supplementary Material 6.
Supplementary Material 7.
Supplementary Material 8.
Supplementary Material 9.
Supplementary Material 10.

Acknowledgements

We sincerely thank the laboratory colleagues and animal facility staff for their invaluable support in research development and discussions of the results. In addition, we thank Daniel Meza and Javier Valdés for developing the fibrinogen-depleted hPL production protocol. Likewise, we express our gratitude to Marcelo Brante, Celeny Figuera, Nadia González, and Yaneisi Vázquez for their invaluable assistance in generating clinical grade sEV. We sincerely thank Diego Castro for his support in project management throughout this research and Dr. Fernando Figuerola for critical discussion of the project objective and clinical setting. We also thank the Experimental Platform Bio-CT, Faculty of Dentistry from Universidad de Chile (ANID Fondecyp #EQM150010) and Daniela Poblete for performing the μ CT analysis.

Author contributions

Alíosa I Figuerola-Valdés Data curation; investigation; formal analysis; methodology; project administration; Conceptualization; supervision; writing—review and editing Patricia Luz-Crawford Data curation; investigation; formal analysis; methodology; conceptualization; writing—review and editing

and funding acquisition. Yeimi Herrera-Luna investigation; formal analysis; methodology Nicolás Georges investigation; formal analysis; methodology; writing—review and editing Cynthia García in vivo investigation; in vivo formal analysis; methodology Hugo E. Tobar investigation; formal analysis; methodology María Jesús Araya investigation; formal analysis; methodology Jose Matas methodology Darío Donoso-Meneses investigation; formal analysis; methodology Catalina de la Fuente investigation; formal analysis; methodology; in vivo investigation Jimena Cuenca Data curation; investigation; formal analysis; methodology Eliseo Parra investigation; formal analysis; methodology Fernando Lillo investigation; formal analysis; methodology Cristóbal Varela, investigation; formal analysis; methodology María Ignacia Cádiz Data curation; methodology Rolando Vernal investigation; in vivo formal analysis; methodology Alexander Ortloff investigation; in vivo formal analysis; methodology Gino Nardocci: Data curation; software; formal analysis; methodology, writing—review and editing Verónica Castañeda Data curation; software; formal analysis; methodology Catalina Adasme-Vidal investigation; formal analysis; methodology Maximiliano Kunze-Küllmer Data curation; methodology Yesenia Hidalgo investigation; formal analysis; methodology Francisco Espinoza methodology Maroun Khoury project administration; funding acquisition; resources; supervision; writing—review and editing Francisca Alcayaga-Miranda: Data curation; investigation; formal analysis; methodology; writing—original draft; project administration; Conceptualization; funding acquisition; resources; supervision; writing—review and editing; validation.

Funding

This research was supported by the National Agency for Research and Development (ANID): Basal funding for Scientific and Technological Center of Excellence, IMPACT #FB210024; Fondecyt Regular #1211376; Fondecyt Regular #1211353; Fondef ID23110325, ID2110194; and Subdirección de Capital Humano/Becas Doctorado Nacional/2022-21220451, 2022-21220015, 2022-21220091, 2023-21230162, and 2022-21220897. Also, CONSORCIO REGENERO “The Chilean Stem Cell and Regenerative Medicine Consortium” CORFO #13CTI-21522; FAI-UANDES (INV-PR-2023-1); and Cells for Cells S.A.

Availability of data and materials

The authors declare that the data supporting the findings of this study are available within the paper and its Supplementary Information files. If raw data files in another format or any other material is needed, it can be requested from the corresponding authors upon reasonable request.

Declarations

Ethics approval and consent to participate

All the procedures presented in this work were approved by the Ethics Committee of Universidad de los Andes (CEC) and/or by Scientific Ethical Committee of the public agency *Servicio de Salud Metropolitano Oriente* (CESSMO) as indicated throughout the manuscript. Specifically, the following certificates of approval were obtained: CECSSMO050612 for donation of UC-MSC, CEC2021077 for human-derived cells used in vitro studies, CEC201861 for clinical-grade production of UC-MSC and CECSSMO030821 for patient recruitment and intra-articular sEV administration. Informed consent was obtained from all individual participants included in the study.

Consent for publication

All individual participants signed informed consent regarding publishing their data derived from the research.

Competing interests

MK-K, FA-M, MK, and JC received stipends from Cells for Cells S.A. MK is the Chief Scientific Officer of Cells for Cells S.A. and EVast Bio; MK-K is an executive at EVast Bio. AIF-V, FA-M, and MK are inventors of the patent No. PCT/CL2022/05003931. The other authors indicated no potential conflicts of interest.

Author details

¹Laboratorio de Medicina Nano-Regenerativa, Centro de Investigación e Innovación Biomédica (CiIB), Universidad de los Andes, Santiago, Chile. ²Laboratorio de Inmunología Celular y Molecular, Centro de Investigación e Innovación Biomédica (CiIB), Universidad de los Andes, Santiago, Chile. ³Laboratorio de Biología Molecular y Bioinformática, Centro de Investigación e Innovación

Biomédica (CiiB), Universidad de los Andes, Santiago, Chile. ⁴Programa de Doctorado en Biomedicina, Facultad de Medicina, Universidad de los Andes, Santiago, Chile. ⁵Consorcio REGENERO, Chilean Consortium for Regenerative Medicine, Santiago, Chile. ⁶IMPACT, Center of Interventional Medicine for Precision and Advanced Cellular Therapy, Santiago, Chile. ⁷Laboratorio de Biología Periodontal, Facultad de Odontología, Universidad de Chile, Santiago, Chile. ⁸Departamento de Ciencias Veterinarias y Salud Pública, Facultad de Recursos Naturales, Universidad Católica de Temuco, Temuco, Chile. ⁹Centro de Terapia Celular, Clínica Universidad de los Andes, Santiago, Chile. ¹⁰Departamento de Cirugía Ortopédica, Clínica Universidad de los Andes, Santiago, Chile. ¹¹Departamento de Radiología, Clínica Universidad de los Andes, Santiago, Chile. ¹²Departamento de Reumatología, Clínica Universidad de los Andes, Santiago, Chile. ¹³Cells for Cells, Santiago, Chile. ¹⁴Evast Bio, Miami, FL, USA. ¹⁵Escuela de Medicina, Facultad de Medicina, Universidad de los Andes, Santiago, Chile.

Received: 25 June 2024 Accepted: 30 December 2024

Published online: 13 January 2025

References

- Albanese M, Chen Y-FA, Hüls C, Gärtner K, Tagawa T, Mejias-Perez E, Keppeler OT, Göbel C, Zeidler R, Shein M, Schütz AK, Hammerschmidt W. MicroRNAs are minor constituents of extracellular vesicles that are rarely delivered to target cells. *PLoS Genet*. 2021;17(12): e1009951. <https://doi.org/10.1371/journal.pgen.1009951>.
- Alcayaga-Miranda F, González PL, Lopez-Verrilli A, Varas-Godoy M, Aguilera-Díaz C, Contreras L, Khoury M. Prostate tumor-induced angiogenesis is blocked by exosomes derived from menstrual stem cells through the inhibition of reactive oxygen species. *Oncotarget*. 2016;7(28):44462–77. <https://doi.org/10.18632/oncotarget.9852>.
- Ansari MY, Ahmad N, Haqqi TM. Oxidative stress and inflammation in osteoarthritis pathogenesis: role of polyphenols. *Biomed Pharmacother*. 2020;129: 110452. <https://doi.org/10.1016/j.biopha.2020.110452>.
- Baietti MF, Zhang Z, Mortier E, Melchior A, Degeest G, Geeraerts A, Ivarsson Y, Depoortere F, Coomans C, Vermeiren E, Zimmermann P, David G. Syndecan-syntenin-ALIX regulates the biogenesis of exosomes. *Nat Cell Biol*. 2012;14(7):677–85. <https://doi.org/10.1038/ncb2502>.
- Banerjee S, Cui H, Xie N, Tan Z, Yang S, Icyuz M, Thannickal VJ, Abraham E, Liu G. miR-125a-5p regulates differential activation of macrophages and inflammation. *J Biol Chem*. 2013;288(49):35428–36. <https://doi.org/10.1074/jbc.M112.426866>.
- Bertolino GM, Maumus M, Jorgensen C, Noël D. Therapeutic potential in rheumatic diseases of extracellular vesicles derived from mesenchymal stromal cells. *Nat Rev Rheumatol*. 2023;19(11):682–94. <https://doi.org/10.1038/s41584-023-01010-7>.
- Le Blanc K, Tammik C, Rosendahl K, Zetterberg E, Ringdén O. HLA expression and immunologic properties of differentiated and undifferentiated mesenchymal stem cells. *Exp Hematol*. 2003;31(10):890–6. [https://doi.org/10.1016/s0301-472x\(03\)00110-3](https://doi.org/10.1016/s0301-472x(03)00110-3).
- Boulestreau J, Maumus M, Jorgensen C, Noël D. Extracellular vesicles from mesenchymal stromal cells: Therapeutic perspectives for targeting senescence in osteoarthritis. *Adv Drug Deliv Rev*. 2021;175: 113836. <https://doi.org/10.1016/j.addr.2021.113836>.
- Cell-Based Regenerative Endodontics for Treatment of Periapical Lesions: A randomized controlled phase I/II clinical trial *Journal of Dental Research*. 2020; 99(5):523–29. <https://doi.org/10.1177/0022034520913242>.
- Chaintreuil P, Kerreneur E, Bourgoin M, Savy C, Favreau C, Robert G, Jacquelin A, Auberger P. The generation, activation, and polarization of monocyte-derived macrophages in human malignancies. *Front Immunol*. 2023;14:1178337. <https://doi.org/10.3389/fimmu.2023.1178337>.
- Chang L, Xia J. MicroRNA regulatory network analysis using miRNet 2.0. *Method Mol Biol* (Clifton NJ). 2023a;2594:185–204. https://doi.org/10.1007/978-1-0716-2815-7_14.
- Chen P, Tang S, Gao H, Zhang H, Chen C, Fang Z, Peng G, Weng H, Chen A, Zhang C, Qiu Z, Li S, Chen J, Chen L, Chen X. Wharton's jelly mesenchymal stem cell-derived small extracellular vesicles as natural nanoparticles to attenuate cartilage injury via microRNA regulation. *Int J Pharm*. 2022;623: 121952. <https://doi.org/10.1016/j.ijpharm.2022.121952>.
- Cosenza S, Ruiz M, Toupet K, Jorgensen C, Noël D. Mesenchymal stem cells derived exosomes and microparticles protect cartilage and bone from degradation in osteoarthritis. *Sci Rep*. 2017;7(1):16214. <https://doi.org/10.1038/s41598-017-15376-8>.
- Cui A, Li H, Wang D, Zhong J, Chen Y, Lu H. Global, regional prevalence, incidence and risk factors of knee osteoarthritis in population-based studies. *Eclinicalmedicine*. 2020;29–30: 100587. <https://doi.org/10.1016/j.eclinm.2020.100587>.
- Cui C, Zhong B, Fan R, Cui Q. HMDD v4.0: a database for experimentally supported human microRNA-disease associations. *Nucl Acid Res*. 2024. <https://doi.org/10.1093/nar/gkad717>.
- Dominici M, Le Blanc K, Mueller I, Slaper-Cortenbach I, Marini F, Krause D, Deans R, Keating A, Prockop D, Horwitz E. Minimal criteria for defining multipotent mesenchymal stromal cells. The international society for cellular therapy position statement. *Cytotherapy*. 2006;8(4):315–7.
- FDA/CBER. Considerations for the design of early-phase clinical trials of cellular and gene therapy products. Guidance for Industry. U.S. Department of Health and Human Services, Food and Drug Administration, Center for Biologics Evaluation and Research, June 2015. Retrieved April 1, 2024, from <https://www.fda.gov/media/106369/download>
- Falcon S, Gentleman R. Using GOstats to test gene lists for GO term association. *Bioinformatics* (Oxford England). 2007;23(2):257–8. <https://doi.org/10.1093/bioinformatics/btl567>.
- Fernandes TL, Gomoll AH, Lattermann C, Hernandez AJ, Bueno DF, Amano MT. Macrophage: a potential target on cartilage regeneration. *Front Immunol*. 2020;11:111. <https://doi.org/10.3389/fimmu.2020.00111>.
- Figuroa-Valdés AI, de la Fuente C, Hidalgo Y, Vega-Letter AM, Tapia-Limonchi R, Khoury M, Alcayaga-Miranda F. A chemically defined, xeno- and blood-free culture medium sustains increased production of small extracellular vesicles from mesenchymal stem cells. *Front Bioeng Biotechnol*. 2021. <https://doi.org/10.3389/fbioe.2021.619930>.
- Fortunato O, Borzi C, Milione M, Centonze G, Conte D, Boeri M, Verri C, Moro M, Facchinetti F, Andriani F, Roz L, Caleca L, Huber V, Cova A, Camisaschi C, Castelli C, Cancila V, Tripodo C, Pastorino U, Sozzi G. Circulating mir-320a promotes immunosuppressive macrophages M2 phenotype associated with lung cancer risk. *Int J Cancer*. 2019;144(11):2746–61. <https://doi.org/10.1002/ijc.31988>.
- GBD 2021 Osteoarthritis Collaborators. Global, regional, and national burden of osteoarthritis, 1990–2020 and projections to 2050: a systematic analysis for the Global Burden of Disease Study 2021. *Lancet Rheumatol*. 2023;5(9):e508–22. [https://doi.org/10.1016/S2665-9913\(23\)00163-7](https://doi.org/10.1016/S2665-9913(23)00163-7).
- González PL, Carvajal C, Cuenca J, Alcayaga-Miranda F, Figuroa FE, Bartolucci J, Salazar-Aravena L, Khoury M. Chorion mesenchymal stem cells show superior differentiation, immunosuppressive, and angiogenic potentials in comparison with haploidentical maternal placental cells. *Stem Cells Transl Med*. 2015;4(10):1109–21. <https://doi.org/10.5966/sctm.2015-0022>.
- Gore M, Tai KS, Sadosky A, Leslie D, Stacey BR. Clinical comorbidities, treatment patterns, and direct medical costs of patients with osteoarthritis in usual care: a retrospective claims database analysis. *J Med Econ*. 2011;14(4):497–507. <https://doi.org/10.3111/13696998.2011.594347>.
- Graff JW, Dickson AM, Clay G, McCaffrey AP, Wilson ME. Identifying functional microRNAs in macrophages with polarized phenotypes. *J Biol Chem*. 2012;287(26):21816–25. <https://doi.org/10.1074/jbc.M111.327031>.
- Hardcastle SA, Dieppe P, Gregson CL, Davey Smith G, Tobias JH. Osteoarthritis and bone mineral density: are strong bones bad for joints? *BoneKey Rep*. 2015;4:624. <https://doi.org/10.1038/bonekey.2014.119>.
- Henrotin YE, Bruckner P, Pujol JPL. The role of reactive oxygen species in homeostasis and degradation of cartilage. *Osteoarthritis Cartil*. 2003;11(10):747–55. [https://doi.org/10.1016/s1063-4584\(03\)00150-x](https://doi.org/10.1016/s1063-4584(03)00150-x).
- Hwang HS, Kim HA. Chondrocyte apoptosis in the pathogenesis of osteoarthritis. *Int J Mol Sci*. 2015;16(11):26035–54. <https://doi.org/10.3390/ijms161125943>.

29. Héraud F, Héraud A, Harmand MF. Apoptosis in normal and osteoarthritic human articular cartilage. *Ann Rheum Dis*. 2000;59(12):959–65. <https://doi.org/10.1136/ard.59.12.959>.
30. Jorge, Bartolucci Fernando J, Verdugo Paz L, González Ricardo E, Larrea Ema, Abarzua Carlos, Goset Pamela, Rojo Ivan, Palma Ruben, Lamich Pablo A, Pedreras Gloria, Valdivia Valentina M, Lopez Carolina, Nazzal Francisca, Alcayaga-Miranda Jimena, Cuenca Matthew J, Brobeck Amit N, Patel Fernando E, Figueroa Maroun, Khoury. Safety and Efficacy of the Intravenous Infusion of Umbilical Cord Mesenchymal Stem Cells in Patients With Heart Failure *Circulation Research*. 2017;121(10):1192–204. <https://doi.org/10.1161/CIRCRESAHA.117.310712>
31. Khoury M, Alcayaga-Miranda F, Figueroa-Valdés AI. Extracellular vesicles of umbilical cord mesenchymal cells for treating osteoarticular and autoimmune diseases. 2022. <https://patentimages.storage.googleapis.com/6e/a1/42/f27a775dcd44f5/WO2022221969A1.pdf>.
32. Kolasinski SL, Neogi T, Hochberg MC, Oatis C, Guyatt G, Block J, Callahan L, Copenhaver C, Dodge C, Felson D, Gellar K, Harvey WF, Hawker G, Herzig E, Kwoh CK, Nelson AE, Samuels J, Scanzello C, White D, Reston J. 2019 American college of rheumatology/arthritis foundation guideline for the management of osteoarthritis of the hand, hip, and knee. *Arthritis Rheumatol* (Hoboken, NJ). 2020;72(2):220–33. <https://doi.org/10.1002/art.41142>.
33. Kordelas L, Rebmann V, Ludwig AK, Radtke S, Ruesing J, Doepfner TR, Epple M, Horn PA, Beelen DW, Giebel B. MSC-derived exosomes: a novel tool to treat therapy-refractory graft-versus-host disease. *Leukemia*. 2014;28(4):970–3. <https://doi.org/10.1038/leu.2014.41>.
34. Kovarik P, Stoiber D, Novy M, Decker T. Stat1 combines signals derived from IFN- γ and LPS receptors during macrophage activation. *EMBO J*. 1998;17(13):3660–8. <https://doi.org/10.1093/emboj/17.13.3660>.
35. Kraus VB, McDaniel G, Huebner JL, Stabler TV, Pieper CF, Shipes SW, Petry NA, Low PS, Shen J, McNearney TA, Mitchell P. Direct in vivo evidence of activated macrophages in human osteoarthritis. *Osteoarthritis Cartilage*. 2016;24(9):1613–21. <https://doi.org/10.1016/j.joca.2016.04.010>.
36. Kroin JS, Kc R, Li X, Hamilton JL, Das V, Van Wijnen AJ, Dall OM, Shelly DA, Kenworth T, Im HJ. Intraarticular slow-release triamcinolone acetate reduces allodynia in an experimental mouse knee osteoarthritis model. *Gene*. 2016;591(1):1–5. <https://doi.org/10.1016/j.gene.2016.06.049>.
37. Kubala MH, Punj V, Placencio-Hickok VR, Fang H, Fernandez GE, Sposto R, DeClerck YA. Plasminogen activator inhibitor-1 promotes the recruitment and polarization of macrophages in cancer. *Cell Rep*. 2018;25(8):2177–2191.e7. <https://doi.org/10.1016/j.celrep.2018.10.082>.
38. Kumar P, Nagarajan A, Uchil PD. Analysis of cell viability by the lactate dehydrogenase assay. *Cold Spring Harb Protoc*. 2018. <https://doi.org/10.1101/pdb.prot095497>.
39. Lara-Barba E, Araya MJ, Hill CN, Bustamante-Barrientos FA, Orloff A, García C, Galvez-Jiron F, Pradenas C, Luque-Campos N, Maita G, Elizondo-Vega R, Djouad F, Vega-Letter AM, Luz-Crawford P. Role of microRNA shuttled in small extracellular vesicles derived from mesenchymal stem/stromal cells for osteoarticular disease treatment. *Front Immunol*. 2021. <https://doi.org/10.3389/fimmu.2021.768771>.
40. Lener T, Gimona M, Aigner L, Börger V, Buzas E, Camussi G, Chaput N, Chatterjee D, Court FA, del Portillo HA, O'Driscoll L, Fais S, Falcon-Perez JM, Felderhoff-Mueser U, Fraile L, Gho YS, Görgens A, Gupta RC, Hendrix A, Giebel B. Applying extracellular vesicles based therapeutics in clinical trials—an ISEV position paper. *J Extracell Vesicles*. 2015. <https://doi.org/10.3402/jev.v4.30087>.
41. Lepetsos P, Papavassiliou AG. ROS/oxidative stress signaling in osteoarthritis. *Biochem Biophys Acta*. 2016;1862(4):576–91. <https://doi.org/10.1016/j.bbadis.2016.01.003>.
42. Li K, Yan G, Huang H, Zheng M, Ma K, Cui X, Lu D, Zheng L, Zhu B, Cheng J, Zhao J. Anti-inflammatory and immunomodulatory effects of the extracellular vesicles derived from human umbilical cord mesenchymal stem cells on osteoarthritis via M2 macrophages. *J Nanobiotechnol*. 2022;20(1):38. <https://doi.org/10.1186/s12951-021-01236-1>.
43. Liu B, Zhang M, Zhao J, Zheng M, Yang H. Imbalance of M1/M2 macrophages is linked to severity level of knee osteoarthritis. *Exp Ther Med*. 2018;16(6):5009–14. <https://doi.org/10.3892/etm.2018.6852>.
44. Loeser RF, Collins JA, Diekmann BO. Ageing and the pathogenesis of osteoarthritis. *Nat Rev Rheumatol*. 2016;12(7):412–20. <https://doi.org/10.1038/nrrheum.2016.65>.
45. Loor G, Kondapalli J, Schriewer JM, Chandel NS, Vanden Hoek TL, Schumacker PT. Menadione triggers cell death through ROS-dependent mechanisms involving PARP activation without requiring apoptosis. *Free Radical Biol Med*. 2010;49(12):1925–36. <https://doi.org/10.1016/j.freeradbiomed.2010.09.021>.
46. Marchev AS, Dimitrova PA, Burns AJ, Kostov RV, Dinkova-Kostova AT, Georgiev MI. Oxidative stress and chronic inflammation in osteoarthritis: can NRF2 counteract these partners in crime? *Ann N Y Acad Sci*. 2017;1401(1):114–35. <https://doi.org/10.1111/nyas.13407>.
47. Matas J, García C, Poblete D, Vernal R, Orloff A, Luque-Campos N, Hidalgo Y, Cuenca J, Infante C, Cadiz MI, Khoury M, Luz-Crawford P, Espinoza F. A phase I dose-escalation clinical trial to assess the safety and efficacy of umbilical cord-derived mesenchymal stromal cells in knee osteoarthritis. *Stem Cells Transl Med*. 2024;13(3):193–203. <https://doi.org/10.1093/stcltm/szad088>.
48. Matas J, Orrego M, Amenabar D, Infante C, Tapia-Limonchi R, Cadiz MI, Alcayaga-Miranda F, González PL, Muse E, Khoury M, Figueroa FE, Espinoza F. Umbilical cord-derived mesenchymal stromal cells (MSCs) for knee osteoarthritis: repeated MSC dosing is superior to a single MSC dose and to hyaluronic acid in a controlled randomized phase I/II trial. *Stem Cells Transl Med*. 2019;8(3):215–24. <https://doi.org/10.1002/sctm.18-0053>.
49. Mathilde, Mathieu Lorena, Martin-Jaular Grégory, Lavieau Clotilde, Théry. Specificities of secretion and uptake of exosomes and other extracellular vesicles for cell-to-cell communication *Nature Cell Biology*. 2019;21(1):9–17. <https://doi.org/10.1038/s41556-018-0250-9>.
50. Maumus M, Noël D, Ea HK, Moulin D, Ruiz M, Hay E, Houard X, Cleret D, Cohen-Solal M, Jacques C, Jouzeau J-Y, Lafage-Proust M-H, Reboul P, Sellam J, Vinatier C, Rannou F, Jorgensen C, Guicheux J, Berenbaum F. Identification of TGF β signatures in six murine models mimicking different osteoarthritis clinical phenotypes. *Osteoarthritis Cartilage*. 2020;28(10):1373–84. <https://doi.org/10.1016/j.joca.2020.06.008>.
51. McKenna MT, Michaud CM, Murray CJL, Marks JS. Assessing the burden of disease in the United States using disability-adjusted life years. *Am J Prev Med*. 2005;28(5):415–23. <https://doi.org/10.1016/j.amepre.2005.02.009>.
52. Molthen RC, Jameson J, Albert C, Smith P, Harris GF. Role of micro-CT in the visualization, measurement, and quantification of bone structure in osteogenesis imperfecta. In: Molthen RC, Jameson J, Albert C, Smith P, Harris GF, editors. *Biomedical engineering faculty research and publications*. Chicago: Shriners Hospitals for Children-Chicago; 2016. p. 195–216.
53. Morita K, Miyamoto T, Fujita N, Kubota Y, Ito K, Takubo K, Miyamoto K, Ninomiya K, Suzuki T, Iwasaki R, Yagi M, Takaishi H, Toyama Y, Suda T. Reactive oxygen species induce chondrocyte hypertrophy in endochondral ossification. *J Exp Med*. 2007;204(7):1613–23. <https://doi.org/10.1084/jem.2006.2525>.
54. Moritake A, Kawao N, Okada K, Tatsumi K, Ishida M, Okumoto K, Matsuo O, Akagi M, Kaji H. Plasminogen activator inhibitor-1 deficiency enhances subchondral osteopenia after induction of osteoarthritis in mice. *BMC Musculoskelet Disord*. 2017;18(1):392. <https://doi.org/10.1186/s12891-017-1752-5>.
55. Mortati L, de Girolamo L, Perucca Orfei C, Viganò M, Brayda-Bruno M, Ragni E, Colombini A. In vitro study of extracellular vesicles migration in cartilage-derived osteoarthritis samples using real-time quantitative multimodal nonlinear optics imaging. *Pharmaceutics*. 2020. <https://doi.org/10.3390/pharmaceutics12080734>.
56. Morton DB, Griffiths PH. Guidelines on the recognition of pain, distress and discomfort in experimental animals and an hypothesis for assessment. *Vet Rec*. 1985;116(16):431–6. <https://doi.org/10.1136/vr.116.16.431>.
57. Moskowitz RW. Osteoarthritis cartilage histopathology: grading and staging. *Osteoarthritis Cartilage*. 2006;14(1):1–2. <https://doi.org/10.1016/j.joca.2005.08.015>.
58. Muthu S, Korpershoek JV, Novais EJ, Tawy GF, Hollander AP, Martin I. Failure of cartilage regeneration: emerging hypotheses and related therapeutic strategies. *Nat Rev Rheumatol*. 2023;19(7):403–16. <https://doi.org/10.1038/s41584-023-00979-5>.
59. Nassar W, El-Ansary M, Sabry D, Mostafa MA, Fayad T, Kotb E, Temraz M, Saad AN, Essa W, Adel H. Umbilical cord mesenchymal stem cells derived extracellular vesicles can safely ameliorate the progression of

- chronic kidney diseases. *Biomater Res.* 2016;20:21. <https://doi.org/10.1186/s40824-016-0068-0>.
60. Ni Z, Zhou S, Li S, Kuang L, Chen H, Luo X, Ouyang J, He M, Du X, Chen L. Exosomes: roles and therapeutic potential in osteoarthritis. *Bone Res.* 2020;8:25. <https://doi.org/10.1038/s41413-020-0100-9>.
 61. Pereira C, Guede D, Durães C, Brandão I, Silva N, Passos E, Bernardes M, Monteiro R, Martins MJ. Differential modulation of cancellous and cortical distal femur by fructose and natural mineral-rich water consumption in Ovariectomized female Sprague Dawley rats. *Nutrients.* 2019. <https://doi.org/10.3390/nu11102316>.
 62. du Plessis A, Broeckhoven C, Guelpa A, le Roux SG. Laboratory x-ray micro-computed tomography: a user guideline for biological samples. *GigaScience.* 2017;6(6):1–11. <https://doi.org/10.1093/gigascience/gix027>.
 63. Pritzker KPH, Gay S, Jimenez SA, Ostergaard K, Pelletier J-P, Revell PA, Salter D, van den Berg WB. Osteoarthritis cartilage histopathology: grading and staging. *Osteoarthr Cartil.* 2006;14(1):13–29. <https://doi.org/10.1016/j.joca.2005.07.014>.
 64. Qian J, Fu P, Li S, Li X, Chen Y, Lin Z. miR-107 affects cartilage matrix degradation in the pathogenesis of knee osteoarthritis by regulating caspase-1. *J Orthop Surg Res.* 2021;16(1):40. <https://doi.org/10.1186/s13018-020-02121-7>.
 65. Rackwitz L, Djouad F, Janjanin S, Nöth U, Tuan RS. Functional cartilage repair capacity of de-differentiated, chondrocyte- and mesenchymal stem cell-laden hydrogels in vitro. *Osteoarthr Cartil.* 2014;22(8):1148–57. <https://doi.org/10.1016/j.joca.2014.05.019>.
 66. Rasmuson I. Immune modulation by mesenchymal stem cells. *Exp Cell Res.* 2006;312(12):2169–79. <https://doi.org/10.1016/j.yexcr.2006.03.019>.
 67. Rohde E, Pachler K, Gimona M. Manufacturing and characterization of extracellular vesicles from umbilical cord-derived mesenchymal stromal cells for clinical testing. *Cytotherapy.* 2019;21(6):581–92. <https://doi.org/10.1016/j.jcyt.2018.12.006>.
 68. Romanelli P, Bieler L, Scharler C, Pachler K, Kreutzer C, Zaunmair P, Jakubecova D, Mrowetz H, Benedetti B, Rivera FJ, Aigner L, Rohde E, Gimona M, Strunk D, Couillard-Despres S. Extracellular vesicles can deliver anti-inflammatory and anti-scarring activities of mesenchymal stromal cells after spinal cord injury. *Front Neurol.* 2019;10:1225. <https://doi.org/10.3389/fneur.2019.01225>.
 69. Rosenberger L, Ezquer M, Lillo-Vera F, Pedraza PL, Ortúzar MI, González PL, Figuroa-Valdés AI, Cuenca J, Ezquer F, Khoury M, Alcayaga-Miranda F. Stem cell exosomes inhibit angiogenesis and tumor growth of oral squamous cell carcinoma. *Sci Rep.* 2019. <https://doi.org/10.1038/s41598-018-36855-6>.
 70. Ruiz M, Toupet K, Maumus M, Rozier P, Jorgensen C, Noël D. TGFBI secreted by mesenchymal stromal cells ameliorates osteoarthritis and is detected in extracellular vesicles. *Biomaterials.* 2020;226: 119544. <https://doi.org/10.1016/j.biomaterials.2019.119544>.
 71. Ryan JM, Barry FP, Murphy JM, Mahon BP. Mesenchymal stem cells avoid allogeneic rejection. *J Inflamm (London England).* 2005;2:8. <https://doi.org/10.1186/1476-9255-2-8>.
 72. Rószter T. Understanding the mysterious M2 macrophage through activation markers and effector mechanisms. *Mediat Inflamm.* 2015;2015: 816460. <https://doi.org/10.1155/2015/816460>.
 73. Sanchez-Lopez E, Coras R, Torres A, Lane NE, Guma M. Synovial inflammation in osteoarthritis progression. *Nat Rev Rheumatol.* 2022;18(5):258–75. <https://doi.org/10.1038/s41584-022-00749-9>.
 74. Sawchuk SJ, Boivin GP, Duwel LE, Ball W, Bove K, Trapnell B, Hirsch R. Anti-T cell receptor monoclonal antibody prolongs transgene expression following adenovirus-mediated in vivo gene transfer to mouse synovium. *Hum Gene Ther.* 1996;7(4):499–506. <https://doi.org/10.1089/hum.1996.7.4-499>.
 75. Scanzello CR. Role of low-grade inflammation in osteoarthritis. *Curr Opin Rheumatol.* 2017;29(1):79–85. <https://doi.org/10.1097/BOR.0000000000000353>.
 76. Schmitz N, Laverty S, Kraus VB, Aigner T. Basic methods in histopathology of joint tissues. *Osteoarthr Cartil.* 2010;18(Suppl 3):S113–6. <https://doi.org/10.1016/j.joca.2010.05.026>.
 77. Soler R, Orozco L, Munar A, Huguet M, López R, Vives J, Coll R, Codinach M, Garcia-Lopez J. Final results of a phase I-II trial using ex vivo expanded autologous mesenchymal stromal cells for the treatment of osteoarthritis of the knee confirming safety and suggesting cartilage regeneration. *Knee.* 2016;23(4):647–54. <https://doi.org/10.1016/j.knee.2015.08.013>.
 78. Suzuki F, Loucas BD, Ito I, Asai A, Suzuki S, Kobayashi M. Survival of mice with gastrointestinal acute radiation syndrome through control of bacterial translocation. *J Immunol (Baltimore Md 1950).* 2018;201(1):77–86. <https://doi.org/10.4049/jimmunol.1701515>.
 79. Théry C, Witwer KW, Aikawa E, Alcaraz MJ, Anderson JD, Andriantsitohaina R, Antoniou A, Arab T, Archer F, Atkin-Smith GK, Ayre DC, Bach JM, Bachurski D, Baharvand H, Balaj L, Baldacchino S, Bauer NN, Baxter AA, Bebawy M, Zuba-Surma EK. Minimal information for studies of extracellular vesicles 2018 (MISEV2018): a position statement of the International Society for Extracellular Vesicles and update of the MISEV2014 guidelines. *J Extracell Vesicles.* 2018. <https://doi.org/10.1080/20013078.2018.1535750>.
 80. Toh WS, Yarani R, El Andaloussi S, Cho BS, Choi C, Corteling R, De Fougères A, Gimona M, Herz J, Khoury M, Robbins PD, Williams D, Weiss DJ, Rohde E, Giebel B, Lim SK. A report on the International Society for Cell & Gene Therapy 2022 scientific signature series, “therapeutic advances with native and engineered human extracellular vesicles.” *Cytotherapy.* 2023;25(8):810–4. <https://doi.org/10.1016/j.jcyt.2023.02.009>.
 81. Toupet K, Maumus M, Luz-Crawford P, Lombardo E, Lopez-Belmonte J, van Lent P, Garin MI, van den Berg W, Dalemans W, Jorgensen C, Noël D. Survival and biodistribution of xenogenic adipose mesenchymal stem cells is not affected by the degree of inflammation in arthritis. *PLoS ONE.* 2015;10(1): e0114962. <https://doi.org/10.1371/journal.pone.0114962>.
 82. Utomo L, van Osch GJVM, Bayon Y, Verhaar JAN, Bastiaansen-Jenniskens YM. Guiding synovial inflammation by macrophage phenotype modulation: an in vitro study towards a therapy for osteoarthritis. *Osteoarthr Cartil.* 2016;24(9):1629–38. <https://doi.org/10.1016/j.joca.2016.04.013>.
 83. Vandooen J, Itoh Y. Alpha-2-macroglobulin in inflammation, immunity and infections. *Front Immunol.* 2021;12: 803244. <https://doi.org/10.3389/fimmu.2021.803244>.
 84. Wang D, Chai XQ, Hu SS, Pan F. Joint synovial macrophages as a potential target for intra-articular treatment of osteoarthritis-related pain. *Osteoarthr Cartil.* 2022;30(3):406–15. <https://doi.org/10.1016/j.joca.2021.11.014>.
 85. Wang L-X, Zhang S-X, Wu H-J, Rong X-L, Guo J. M2b macrophage polarization and its roles in diseases. *J Leukoc Biol.* 2019;106(2):345–58. <https://doi.org/10.1002/JLB.3RU1018-378RR>.
 86. Warnecke A, Prenzler N, Harre J, Köhl U, Gärtner L, Lenarz T, Laner-Plamberger S, Wietzorrek G, Staecker H, Lassacher T, Hollerweger J, Gimona M, Rohde E. First-in-human intracochlear application of human stromal cell-derived extracellular vesicles. *J Extracell Vesicles.* 2021;10(8): e12094. <https://doi.org/10.1002/jev2.12094>.
 87. Welsh JA, Goberdhan DCI, O’Driscoll L, Buzas EI, Blenkiron C, Bussolati B, Cai H, Di Vizio D, Driedonks TAP, Erdbrügger U, Falcon-Perez JM, Fu QL, Hill AF, Lenassi M, Lim SK, Mahoney MG, Mohanty S, Möller A, Nieuwland R, Witwer KW. Minimal information for studies of extracellular vesicles (MISEV2023): from basic to advanced approaches. *J Extracell Vesicles.* 2024a;13(2): e12404. <https://doi.org/10.1002/jev2.12404>.
 88. William H, Robinson Christin M, Lepus Qian, Wang Harini, Raghu Rong, Mao Tamsin M, Lindstrom Jeremy, Sokolove. Low-grade inflammation as a key mediator of the pathogenesis of osteoarthritis *Nature Reviews Rheumatology.* 2016;12(10):580–92. <https://doi.org/10.1038/nrrheum.2016.136>.
 89. Witwer KW, Van Balkom BWM, Bruno S, Choo A, Dominic M, Gimona M, Hill AF, De Kleijn D, Koh M, Lai RC, Mitsialis SA, Ortiz LA, Rohde E, Asada T, Toh WS, Weiss DJ, Zheng L, Giebel B, Lim SK. Defining mesenchymal stromal cell (MSC)-derived small extracellular vesicles for therapeutic applications. *J Extracell Vesicles.* 2019. <https://doi.org/10.1080/20013078.2019.1609206>.
 90. Woodell-May JE, Sommerfeld SD. Role of inflammation and the immune system in the progression of osteoarthritis. *J Orthop Res Off Publ Orthop Res Soc.* 2020;38(2):253–7. <https://doi.org/10.1002/jor.24457>.
 91. Wright A, Arthaud-Day ML, Weiss ML. Therapeutic use of mesenchymal stromal cells: the need for inclusive characterization guidelines to accommodate all tissue sources and species. *Front Cell Dev Biol.* 2021;9: 632717. <https://doi.org/10.3389/fcell.2021.632717>.

92. Xue C, Tian J, Cui Z, Liu Y, Sun D, Xiong M, Yi N, Wang K, Li X, Wang Y, Xu H, Zhang W, Liang Q. Reactive oxygen species (ROS)-mediated M1 macrophage-dependent nanomedicine remodels inflammatory micro-environment for osteoarthritis recession. *Bioact Mater*. 2024;33:545–61. <https://doi.org/10.1016/j.bioactmat.2023.10.032>.
93. Yu L, Gao Y, Aaron N, Qiang L. A glimpse of the connection between PPAR γ and macrophage. *Front Pharmacol*. 2023;14(August):1–9. <https://doi.org/10.3389/fphar.2023.1254317>.
94. Zavala G, Ramos MP, Figueroa-Valdés AI, Cisternas P, Wyneken U, Hernández M, Toa P, Salmons B, Dangerfield J, Gunzburg WH, Khoury M. Semipermeable cellulose beads allow selective and continuous release of small extracellular vesicles (sEV) from encapsulated cells. *Front Pharmacol*. 2020. <https://doi.org/10.3389/fphar.2020.00679>.
95. Zhang H, Cai D, Bai X. Macrophages regulate the progression of osteoarthritis. *Osteoarthr Cartil*. 2020;28(5):555–61. <https://doi.org/10.1016/j.joca.2020.01.007>.
96. Zhang S, Chuah SJ, Lai RC, Hui JHP, Lim SK, Toh WS. MSC exosomes mediate cartilage repair by enhancing proliferation, attenuating apoptosis and modulating immune reactivity. *Biomaterials*. 2018;156:16–27. <https://doi.org/10.1016/j.biomaterials.2017.11.028>.
97. Zhang J, Rong Y, Luo C, Cui W. Bone marrow mesenchymal stem cell-derived exosomes prevent osteoarthritis by regulating synovial macrophage polarization. *Aging*. 2020;12(24):25138–52. <https://doi.org/10.18632/aging.104110>.
98. Zhang S, Teo KYW, Chuah SJ, Lai RC, Lim SK, Toh WS. MSC exosomes alleviate temporomandibular joint osteoarthritis by attenuating inflammation and restoring matrix homeostasis. *Biomaterials*. 2019;200:35–47. <https://doi.org/10.1016/j.biomaterials.2019.02.006>.
99. Zhang Y, Wei X, Browning S, Scuderi G, Hanna LS, Wei L. Targeted designed variants of alpha-2-macroglobulin (A2M) attenuate cartilage degeneration in a rat model of osteoarthritis induced by anterior cruciate ligament transection. *Arthritis Res Ther*. 2017;19(1):175. <https://doi.org/10.1186/s13075-017-1363-4>.
100. Zhou H, Shen X, Yan C, Xiong W, Ma Z, Tan Z, Wang J, Li Y, Liu J, Duan A, Liu F. Extracellular vesicles derived from human umbilical cord mesenchymal stem cells alleviate osteoarthritis of the knee in mice model by interacting with METTL3 to reduce m6A of NLRP3 in macrophage. *Stem Cell Res Ther*. 2022;13(1):322. <https://doi.org/10.1186/s13287-022-03005-9>.
101. Zhu X, Lee C-W, Xu H, Wang Y-F, Yung PSH, Jiang Y, Lee OK. Phenotypic alteration of macrophages during osteoarthritis: a systematic review. *Arthritis Res Ther*. 2021;23(1):110. <https://doi.org/10.1186/s13075-021-02457-3>.
102. Zhuang Y, Jiang S, Yuan C, Lin K. The potential therapeutic role of extracellular vesicles in osteoarthritis. *Front Bioengin Biotechnol*. 2022;10:1022368. <https://doi.org/10.3389/fbioe.2022.1022368>.

Publisher's Note

Springer Nature remains neutral with regard to jurisdictional claims in published maps and institutional affiliations.